Modelling oxygen and argon to improve estimation of net community productivity in a coastal upwelling zone using $\Delta O_2/Ar$

by

Lianna Teeter
B.Sc., Queen's University, 2011

A Thesis Submitted in Partial Fulfillment of the
Requirements for the Degree of

MASTER OF SCIENCE

in the School of Earth and Ocean Sciences

Modelling oxygen and argon to improve estimation of net community productivity in a coastal upwelling zone using $\Delta O_2/Ar$

by

Lianna Teeter
B.Sc., Queen's University, 2011

Supervisory Committee

Dr. Roberta Hamme, Co-Supervisor
(Associate Professor - School of Earth and Ocean Sciences)

Dr. Debby Ianson, Co-Supervisor
(Adjunct Professor - School of Earth and Ocean Sciences)

Dr. Ken Denman, Departmental Member
(Adjunct Professor - School of Earth and Ocean Sciences)

Supervisory Committee

Dr. Roberta Hamme, Co-Supervisor
(Associate Professor - School of Earth and Ocean Sciences)

Dr. Debby Ianson, Co-Supervisor
(Adjunct Professor - School of Earth and Ocean Sciences)

Dr. Ken Denman, Departmental Member
(Adjunct Professor - School of Earth and Ocean Sciences)

Abstract

Under steady state conditions where the rate of biological oxygen production is balanced by oxygen evasion to the atmosphere, net community production (NCP) can be estimated from mixed layer oxygen/argon measurements. This method is effective in the open ocean but not in coastal zones where upwelling of low oxygen water violates the simple steady state assumption. Since these upwelling regions are highly productive, excluding them can lead to significant underestimations of global productivity. Here, I use a quasi-2D version of the Regional Ocean Modelling System (ROMS), including oxygen and argon as prognostic variables, to model the relationship between NCP and the sea-to-air flux of biological oxygen in a coastal upwelling system. The relationship between the sea-to-air flux of biological oxygen and NCP is poorest near the shore during upwelling favourable winds when waters that are undersaturated in oxygen reach the surface and depress the oxygen/argon ratio. I averaged NCP temporally and spatially over the residence time with respect to gas exchange and the Lagrangian motion of a water parcel. I found that the maximum distance travelled ($\sim$25 km) over this time period indicated a distance from the upwelling plume at which much of the the low oxygen signal is erased. When the sea-to-air flux of biological oxygen was below 20 mmol m^{-2} day^{-1}, NCP was usually also found in that range. Above that range the sea-to-air flux of biological

oxygen is a lower bound for NCP. NCP occurring below the mixed layer can affect the sea-to-air flux of biological oxygen either by entrainment or diffusion into the mixed layer causing an overestimation of NCP, but this process had a minimal effect on most of my model data. Removing values with mixed layers deeper than 25 m improves the estimation, although further studies may reveal that this depth should be adjusted based on mean wind forcing.

Contents

List of Tables

List of Figures

Acknowledgments

First and foremost, I would like to thank my supervisors, Dr. Roberta Hamme and Dr. Debby Ianson, without whom this would not have been possible. They have never failed to be completely supportive and have always been so understanding of the frustrations involved in coding. I've had some amazing opportunities through both of them, and would not have found this branch of science that I enjoy so much without them. I'd also like to thank Ken Denman, the final member of my committee, for his insight and help.

Thanks also go out to Laura Bianucci and Wendy Callendar for walking me through the sometimes frustrating complexity of ROMS when I was drowning in the sheer volume of code. Also to Phil Tortell and the Institute of Ocean Sciences for providing coastal Vancouver Island observations.

My family; Mom, Dad, and Emi of course, who have smiled and nodded and pretended to at least vaguely understand what I do, but who have always unequivocally supported me and my goals even when I decided to move to the other side of the country. I don't know what I would do without them. They have always been there for me through my frustrations and triumphs ready to lend an ear or congratulations or anything in between. I would not be who or where I am today if not for them.

My friends from Ontario who kept me company when I knew no one out here and the friends I've made out here since; Alex, Carolyn, Alyssa, Alisenne, Stefan, Graeme, Becca, James, Chris, Jake, Bren, Caz, Taylor, Erin, Stacey, the Amandas, Leah, and all my fellow SEOS students (there are way too many of you to name). You have all kept me from becoming a complete recluse. My rugby teammates, past and present, have always been there to provide an outlet for frustration, a distraction from the world of code, and in general some absolutely amazing experiences. My gym partner Tanysia needs to get a mention for dragging me to the gym and keeping me sane, especially when rugby was in the off season.

Funding was provided by Climate CREATE, the School of Earth and Ocean Sciences (University of Victoria Graduate Award), and Roberta Hamme's Discovery (DG-329290-2012) and GEOTRACES CCAR grants.

Chapter 1

Introduction

Motivation Biological productivity drives the biological pump, which, along with the solubility pump, is one of two main mechanisms transporting carbon from the surface to the deep ocean (Volk and Hoffert, 1985). Particulate and dissolved organic matter are produced by photosynthesis and then either sink, or undergo mixing, advection, or zooplankton mediated transport, to the deeper ocean. The biological pump is likely not directly affected by the atmospheric concentration of carbon dioxide; however, it accounts for the sequestration of significant amounts of carbon dioxide from the atmosphere (Siegenthaler and Sarmiento, 1993).

Quantifying ocean productivity is important in order to estimate the global uptake of carbon by the oceans (Emerson, 2014). However, despite containing the most productive regions of the global ocean (Harrison et al., 1987), the coastal areas are undersampled as are many regions of the oceans. The heterogeneity of coastal zones is such that many small scale events and processes are missed due to this undersampling. Research on carbon uptake by coastal regions is impeded by this heterogeneity and the lack of CO_2 air-sea flux data in many areas (Cai et al., 2006). Equatorward winds in coastal upwelling zones cause Ekman transport of surface water offshore (Smith, 1994) and draw oxygen poor, carbon and nutrient-rich water to the surface, causing high levels of productivity (Hales et al., 2006; Ianson and Allen, 2002; Nemcek et al., 2008). Therefore, although coastal upwelling zones make up only a small percentage of the global ocean, they are responsible for a high percentage of global productivity (Botsford et al., 2006; Hales et al., 2006).

Coastal upwelling zones are associated with lucrative fisheries. Primary productivity generates phytoplankton biomass which supports higher trophic levels, so high productivity in coastal upwelling zones supports a high percentage of the world's

fish supplies (Ryther, 1986; Ware and Thomson, 2005). Therefore, predictions of upwelling and the corresponding primary productivity can lead to predictions of the abundance of fish supported by a given region (Botsford et al., 2006). If we can use the combination of an upwelling index and measurements of NCP to predict areas capable of supporting high concentrations of fish, it will improve our prediction of the adaptability of fisheries over time (Botsford et al., 2006).

Hypoxia can also be found along the shelf bottom of coastal upwelling zones. High productivity caused by upwelling of water high in nitrate causes particulate organic carbon to sink to the bottom on the shelf. If this carbon is respired locally it further lowers the oxygen concentration in water that is already low in oxygen and may create hypoxic environments (Crawford and Peña, 2013; Hales et al., 2006). If the particulate organic carbon is respired below the mixed layer in the summer, then stormy winter conditions can deepen the mixed layer and release carbon dioxide back to the atmosphere (Barth and Wheeler, 2005) cancelling out the summer uptake of carbon on annual timescales (Ianson et al., 2009).

High upwelling favourable winds can cause advection of the nitrate rich water offshore causing productivity to occur offshore of the shelf break. While this advection can have negative effect on higher trophic levels which depend on onshore production for its production of biomass (Botsford et al., 2006), it can also mean that particulate organic carbon may sink below upwelling source waters causing it to be lost from the short term carbon cycle (Walsh et al., 1991). Improved measures of productivity will greatly increase our understanding of the role of these coastal zones in the carbon cycle, and by extension the sequestration of anthropogenic carbon from the atmosphere into the deep ocean, the effects of these zones on fisheries, and their relationship to hypoxia.

Measurement of NCP using oxygen/argon gas ratios Net community productivity (NCP) is defined as gross photosynthetic oxygen production (GOP) minus oxygen consumption by all organisms and metabolic processes. It is related to a change in the amount of carbon in the mixed layer or carbon export. Over longer timescales the change of carbon in the mixed layer is small and carbon export can be approximated by NCP (Hamme et al., 2012). NCP is expressed in oxygen units in this paper. I also discuss net primary production (NPP), which is defined as gross primary productivity minus respiration by primary producers (Nicholson et al., 2012; Reuer et al., 2007).

NCP can be estimated through the measurement of dissolved oxygen/argon ratios. Since both gases have similar physical properties, their percent saturations would be similar in the absence of biological production and consumption (Kaiser et al., 2005). Argon can therefore be used as a benchmark so that one can estimate what the oxygen concentration would be without biological processes, allowing the isolation of biologically produced oxygen (Kaiser et al., 2005). The sea-to-air flux of biological oxygen determined from the oxygen/argon ratio is equivalent to NCP under steady state conditions i.e.: constant NCP, constant mixed layer depth in a physically isolated region, little or no mixing with water outside of the mixed layer, and no advection (Hamme et al., 2012; Jonsson et al., 2013; Kaiser et al., 2005; Reuer et al., 2007).

The measurement of NCP using oxygen/argon ratios has distinct advantages over other methods used to measure productivity. For example, the uptake of ^{14}C-labelled DIC by the phytoplankton community in bottle incubations (Peterson, 1980; Steemann Nielsen, 1952), which measures primary production (between NPP and GPP) (Giesbrecht et al., 2012), is time consuming and labour intensive. In addition there are uncertainties associated with isolating the biological community in a bottle, which does not exactly replicate *in situ* situations (Giesbrecht et al., 2012; Quay et al., 2010). By contrast, measuring oxygen/argon with an underway mass spectrometer can supply excellent spatial coverage and be standardized by comparison to air ratios (Cassar et al., 2009; Kaiser et al., 2005). Also, the ^{14}C method yields 12 or 24 hour measurements at set locations while oxygen/argon yields more integrated measurements over a period of time ranging from a few days to several weeks depending on the timescales of sea-to-air oxygen fluxes.

Satellites integrate measurements of chlorophyll levels and provide extensive spatial coverage which can be used as a proxy for biological productivity, although the relationship to carbon export is less direct. Chlorophyll levels are not directly related to ^{14}C uptake rates or productivity rates assessed using other methods. Variable carbon:chlorophyll ratios can also be a problem when converting to carbon export. However, chlorophyll and carbon export do correlate allowing chlorophyll to be used as a proxy for biomass (Uitz et al., 2006). Chlorophyll measurements can also be challenging to integrate over longer temporal scales, although Jonsson et al. (2011) suggest a method for integrating over the Lagrangian path of a water parcel using a time series of satellite chlorophyll measurements. This method uses a modelled Lagrangian path to choose images that represent the same parcel of water, and allows for high levels of coverage, but it remains only a proxy for production.

Deriving NCP estimates from oxygen/argon dissolved gas ratios has its own uncertainties. Jonsson et al. (2013) used two biogeochemical ocean circulation models in the Southern Ocean to assess the error in using oxygen/argon ratios to estimate NCP in the open ocean. They found that temporal and spatial misalignment of NCP and the venting of biological oxygen and vertical advection of oxygen across the base of the mixed layer caused significant errors at times. Overall they found that, excluding areas with undersaturated biological oxygen, the sea-to-air flux of biological oxygen underestimates NCP by 5-15% in the Southern Ocean. They also found that biological oxygen measurements in shallow mixed layer depths tended to overestimate NCP in the mixed layer, while measurements in deeper mixed layers tended to underestimate NCP.

In addition to the Jonsson et al. (2013) modelling study in the Southern Ocean, observed oxygen/argon measurements have been used effectively in the open ocean to estimate NCP because conditions are more static over short distances (Emerson et al., 1995; Hendricks et al., 2004; Kaiser et al., 2005; Spitzer and Jenkins, 1989) although submesoscale processes can sometimes generate significant variability (Mahadevan and Tandon, 2006). However, in some coastal and equatorial zones, the upwelling of oxygen undersaturated waters and their mixing with surface waters reduces the oxygen/argon ratio, which causes severe underestimation of NCP until the undersaturated signal has been erased by gas transfer and productivity. In equatorial waters, the upwelling of oxygen poor water from below the mixed layer disrupts the assumption of mass balance necessary for the oxygen/argon method to apply, and all O_2/Ar data within this region are generally discarded (Hendricks et al., 2004; Kaiser et al., 2005; Stanley et al., 2010). Coastal upwelling zones present the same problem with oxygen poor water added to the mixed layer causing a lowering of the oxygen/argon ratio and preventing detection of net community productivity by this method (e.g. large negative values on the California/Oregon border (Ianson et al., 2009)).

Focus As mentioned above, coastal upwelling zones are some of the most productive regions of the world, but are characterized by sporadic bursts of productivity that can be difficult to capture using incubation measurements. For this reason, a method similar to oxygen/argon derived NCP, which integrates productivity over the residence time of gases in the mixed layer, could greatly improve the accuracy of global productivity measurements. I evaluate different algorithms to estimate productivity

from discrete O_2/Ar measurements using a model in coastal upwelling zones, and assess their accuracy. I identify which O_2/Ar data which can be used to accurately predict NCP.

Specifically, I study the relationship between the sea-to-air flux of biological oxygen and NCP in coastal upwelling zones using a quasi-2D (cross shelf vs. depth) model in which NCP is a known flux and can be compared to modelled oxygen and argon fluxes. The model is validated by comparing modelled oxygen and argon supersaturations, and mixed layer depth with observations from a coastal upwelling region. I explore how averaging and weighting methods contribute to the use of oxygen/argon estimates as a proxy for NCP. I also explore at what point the low oxygen upwelling signal is erased in the model domain used, and how generalizable this result is. In addition, I investigate how changes in bathymetry and in wind and radiative forcing affect the results.

Chapter 2

Background

2.1 Biological oxygen supersaturation and biological sea-to-air flux

In a very simple steady state system, net community productivity (NCP) can be derived from the oxygen mass balance. Assuming constant NCP, constant mixed layer depth, and no mixing or advection with water outside the mixed layer, net community production equals diffusive gas exchange. However, other physical processes also affect oxygen in the mixed layer, such as bubble-mediated gas exchange and the effects of temperature change on the solubility of dissolved oxygen. Argon has very similar physical properties to oxygen (solubility, dependence of solubility on pressure and temperature, and molecular diffusion coefficents), and therefore can be used to account for purely physical processes. Any additional oxygen supersaturation relative to argon is therefore due to biological processes and can be used to estimate the sea-to-air flux of biological oxygen, hereafter referred to as bioflux (Jonsson et al., 2013). Argon cannot correct for mixing or entrainment of water below the mixed layer, or for upwelling, which is less of an issue in the open ocean where these factors are usually small, but in coastal upwelling zones they have a much larger effect on the oxygen/argon ratio.

Biological oxygen supersaturation, or the oxygen exceeding equilibrium saturation as a result of biological processes is defined as:

$$\Delta O_2/Ar = \left(\frac{(O_2/Ar)_{meas}}{(O_2/Ar)_{eq}} - 1 \right) \tag{2.1}$$

where $(O_2/Ar)_{meas}$ is the measured dissolved gas concentration ratio and $(O_2/Ar)_{eq}$ is the concentration ratio expected at equilibrium based on potential temperature and salinity. $\Delta O_2/Ar$ is presented in percent (Kaiser et al., 2005). Supersaturation of a single gas (e.g. ΔO_2), defined as the percent concentration above or below the equilibrium concentration, is calculated in a same manner, using the concentrations of the single gas rather than ratios.

Oxygen gas exchange is usually written as the difference between the measured and equilibrium concentrations of oxygen in the mixed layer multiplied by the gas transfer velocity, but using the definition of oxygen supersaturation, that equation can be rearranged:

$$F_{O_2} = k_{O_2}([O_2]_{meas} - [O_2]_{eq}) = k_{O_2} \cdot [O_2]_{eq} \cdot \Delta O_2 \tag{2.2}$$

where F_{O_2} is the air-sea flux of oxygen out of the mixed layer, k_{O_2} is the gas transfer velocity (I used the Ho et al. (2006) parameterization), $[O_2]_{meas}$ is the measured concentration of oxygen in the mixed layer, $[O_2]_{eq}$ is the expected concentration of oxygen in the mixed layer at equilibrium based on salinity and temperature, and ΔO_2 is the supersaturation of oxygen in the mixed layer (Kaiser et al., 2005). The supersaturation multipled by the equilibrium concentration is equal to the difference between the measured and equilibrium concentrations of oxygen. In the same manner, the supersaturation of biological oxygen can be multiplied by the equilibrium concentration of oxygen to calculate bioflux (in units of mmol $m^{-2}day^{-1}$) from the O_2/Ar mass balance;

$$bioflux = k_{O_2} \cdot [O_2]_{eq} \cdot \Delta O_2/Ar \approx NCP \tag{2.3}$$

As discussed above, at steady state bioflux is equivalent to NCP integrated over the mixed layer.

2.2 Gas transfer velocity weighting

To account for recent variability in wind speed on the calculation of bioflux, I weight the gas transfer velocity for oxygen using an adaptation of the 60 day integration method described by Reuer et al. (2007). More recent gas transfer velocities are more highly weighted, but past storm events with higher gas transfer velocities can play a significant role. The weighted gas transfer velocity (k_X) is calculated as:

$$k_X = \frac{\sum_{i=1}^{n} k_i \omega_i}{\sum_{i=1}^{n} \omega_i} \tag{2.4}$$

$$\omega_i = \omega_{i-1}(1 - f_{i-1}) \tag{2.5}$$

$$f_i = k_i \cdot MLD^{-1} \cdot \Delta t, \;\; k_i \Delta t < MLD \tag{2.6}$$

where i is the ith timestep such that i increases going back in time, and f_i is the fraction of the mixed layer ventilated at time i, the inverse of the residence time with respect to gas exchange. The gas transfer velocity, (k_i) is weighted by ω_i such that weighting decreases with time (Equation 2.5), Δt is the timestep, and n is the maximum number of time steps considered. Reuer et al. (2007) chose to extend the calculation over 60 days, a period over which the weighting coefficients drop to near zero under most oceanic conditions. In this work, the mixed layer is likely ventilated in a much shorter time. In order for this method to be stable, $f_i > 0$, meaning that $k_i \Delta t < MLD$. Reuer et al. (2007) multiplied the denominator by $(1 - \omega_n)$ with the intention of accounting for the unventilated portion of the mixed layer previous to the weighting period (60 days in their study). However, if the weighting time is reduced from 60 days, as is appropriate in my region of interest, this term forces the weighted k to grow larger. If the $(1 - \omega_n)$ term is removed, the weighted k maintains similar values at shorter weighting times. At the full 60 days, the difference between including and excluding the $(1 - \omega_n)$ term is less than 1%. Thus, I recommend discarding the $(1 - \omega_n)$ term to give a more accurate weighted gas transfer velocity.

2.3 Bioflux lag

Bioflux (Equation 2.3) is the ventilation of biologically produced oxygen to the atmosphere, however it is not an instantaneous process. The time it takes for oxygen generated by NCP (at a specific point in time and space) to be ventilated to the atmosphere depends on the depth of the mixed layer divided by the weighted gas transfer velocity (Equation 2.6)(Jonsson et al., 2013). For a given gas transfer velocity and supersaturation, a deeper mixed layer (defined here as a region of uniform density) will require more time to ventilate since a larger reservoir of gas must be ventilated with the same sea-to-air flux. At lower wind speeds, the gas transfer velocity is lower and it will also take more time for ventilation to occur. In other words, about 63% $(1 - 1/e)$ of the oxygen that is produced in the mixed layer will be ventilated over

the residence time due to gas exchange, an e-folding time calculated as MLD/k_{O_2}, rather than immediately. Assuming no new addition of oxygen, and given enough time, all the excess oxygen will be ventilated to the atmosphere, and the mixed layer will return to the equilibrium saturation.

Jonsson et al. (2013) demonstrated the time dependent relationship of NCP and bioflux using a simple one box model with constant mixed layer depth and wind speed. I extend their analysis to demonstrate the effect of variable wind speed (Figure 2.1a). My box model assumes a constant 25 m mixed layer depth with no vertical or lateral mixing, variable wind speeds from the summer of 1993 off the west coast of Vancouver island, and forces a bloom with constant NCP lasting 50 days. Temperature and salinity are constant at 20°C and 35, respectively as in Jonsson et al. (2013). Oxygen and argon are initialized at their equilibrium concentrations. In this case, argon concentrations do not change over the model run (due to initialization at equilibrium, no mixing with other waters, and constant temperature), and biological oxygen supersaturation is equivalent to oxygen supersaturation (section 2.1). When the bloom begins, biological oxygen fluxes from the ocean to the atmosphere, based on the typical gas transfer calculation detailed above (Equation 2.3). I show both the instantaneous sea-to-air flux in each model time step that drives the changes in model oxygen inventory (1 hour), and the bioflux calculation using the weighted gas transfer velocity (Equation 2.4-2.6).

Bioflux calculated using the 60 day weighted gas transfer velocity is a smooth curve despite the variability in wind speed and $\Delta O_2/Ar$, and is similar to the results of Jonsson et al. (2013) for constant wind speed (Figure 2.1). The winds are highly variable which leads to the highly variable sea-to-air flux based on the unweighted gas transfer velocity. The concentration of biological oxygen in the mixed layer is affected by the outgassing prior to the day of collection, or to the day being modelled, which in turn affects the gas transfer fluxes. Using the 60 day weighted gas transfer velocity, the bioflux is a smooth curve which eventually reaches the imposed NCP value, fully accounting for the variability in $\Delta O_2/Ar$ (Equation 2.1). If $\Delta O_2/Ar$ in the mixed layer is low, it could mean that NCP is low. However, if there was a large wind event in the recent past, much of the biological oxygen may have already been ventilated to the atmosphere; weighting the gas transfer velocity accounts for this earlier removal.

The gas transfer velocity used in the calculation of bioflux is usually weighted over the past 60 days (Reuer et al., 2007). In this simple model and in my coastal model (section 3.1) there is little difference between the calculated bioflux using k_{O_2} weighted

over 60 days and that estimated using 30 day weighted k_{O_2} (percent difference in the mean k_{O_2} values for 30 and 60 day weighting periods is 3%). It is only when weighting periods fall below ∼20 days that the weighted bioflux begins to deviate from (and fluctuate around) the smooth curve (Figure 2.1c).

2.4 Temporal averaging of NCP

NCP in my box model increases instantly, but bioflux takes several weeks to catch up (Figure 2.1). This mismatch is known as the bioflux lag effect (Jonsson et al., 2013), and can be somewhat accounted for by averaging NCP over a period of days (since NCP is constant, averaging only affects the beginning and end of the bloom). The lower the gas transfer velocity and the deeper the mixed layer, the more time it takes for bioflux to equilibrate with NCP. The forced bloom begins around mid July, and immediately some bioflux occurs as the air-sea flux drives the concentration of oxygen in the mixed layer back towards equilibrium. At the next timestep, the oxygen concentration in the mixed layer has not yet returned to equilibrium and more NCP occurs, driving the oxygen concentration still further from equilibrium. The greater difference between the equilibrium concentration and the actual concentration in the mixed layer increases the bioflux. This increase in outgassing continues until the oxygen flux out of the mixed layer and the flux of NCP into the mixed layer have reached a steady state. When the bloom ends, there is still biological oxygen in the mixed layer, so at each timestep a fraction of the oxygen proportional to the difference between the oxygen concentration in the mixed layer and the equilibrium concentration of oxygen is ventilated to the atmosphere until the mixed layer oxygen concentration reaches equilibrium. At higher wind speeds and shallower mixed layer depths this lag may be only a few timesteps. However, as the wind speed decreases or mixed layer depth increases, the lag effect increases. Averaging NCP over the residence time due to gas exchange accounts for the bioflux lag somewhat in that after the bloom has ended, previous NCP is still taken into account. The 9 day averaged NCP is closer to the bioflux than the flux of NCP into the mixed layer at a given time (instantaneous NCP) (Figure 2.1a)(Jonsson et al., 2013).

I found that weighting of the gas transfer velocity led to a strong estimate of NCP by bioflux when NCP was constant over time. However, in coastal upwelling zones, mixed layer depths can change rapidly, and NCP is not constant, which violates the assumptions of the weighting scheme. The fraction of the mixed layer ventilated is

dependant on mixed layer depth, which is assumed to be constant over the weighting period. As the mixed layer changes, oxygen is entrained or detrained from the mixed layer which also causes changes in the mass balance that are not accounted for by the weighting method (Reuer et al., 2007). The fluctuation of NCP means that bioflux is nearly always overestimating or underestimating NCP. Over a large enough number of measurements, this mismatch should even out since when NCP is increasing, bioflux will tend to underestimate it, but when it is decreasing bioflux tends to overestimate NCP (section 5.3).

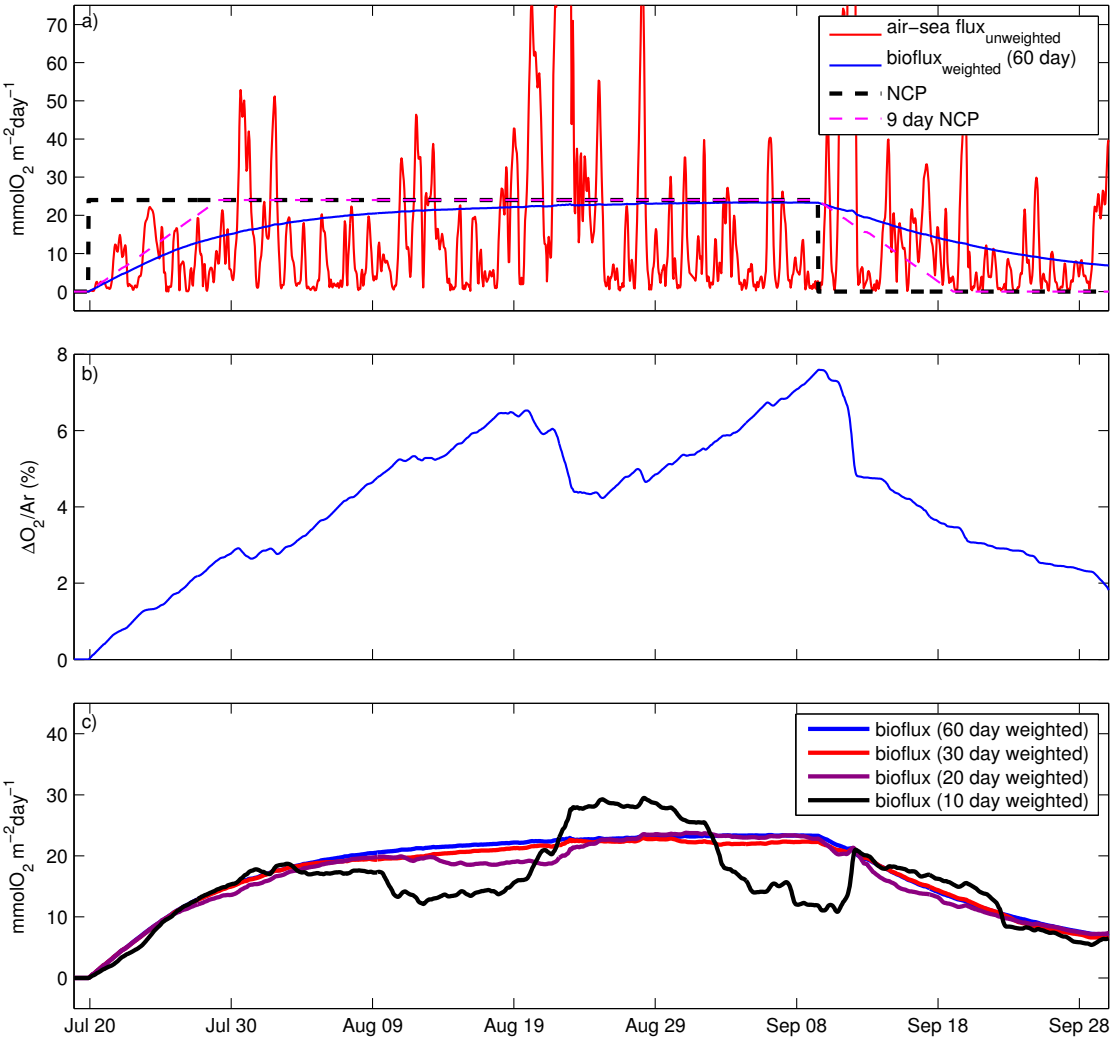

Figure 2.1: a)Single box model in which mixed layer depth is set at 25 m and a bloom with constant NCP of 25 mmol m^{-2} day^{-1} (black dashed line) is forced over a period of 50 days. Wind forcing is calculated from hourly wind data from meteorological buoy 46206 from July 18 to September 29 in 1993. Red and blue lines represent the unweighted sea-to-air flux of biological oxygen and 60 day weighted bioflux, respectively. The magenta dashed line represents NCP averaged over the previous 9 days. b) Biological oxygen supersaturation ($\Delta O_2/Ar$) in the mixed layer. c) Bioflux weighted over 60, 30, 20, and 10 days. Blue line is identical to the 60 day weighted bioflux (blue) in panel a.

Chapter 3

Methods

The model used here is an adaptation of a quasi-2D configuration of the Regional Ocean Modelling System (ROMS) version 3.2 described by Laura Bianucci et al. (2011). This model runs over a 125 day period in summer, so that no model restoring is necessary. Argon was added to the Bianucci et al. (2011) model as a physical tracer that undergoes gas exchange, and the resolution of vertical boxes was increased at the surface in order to more accurately portray mixed layer dynamics. Oxygen and argon concentrations were then used to calculate the sea-to-air flux of biological oxygen (bioflux) as a proxy for NCP.

3.1 Model specifications

3.1.1 Physical Model

The ROMS kernel is described by Shchepetkin and McWilliams (2005), while the quasi-2D version of the model used here represents wind-driven upwelling in a cross-shelf vs depth domain with uniform properties in the alongshore dimension (Bianucci et al., 2011). Periodic open boundary conditions allow the conditions alongshore to remain uniform - what goes out at one edge of the model in the alongshore direction comes back in at the other edge. Offshore boundary conditions are set as open boundary, although I do not interpret model data within 100 km of the offshore boundary. The model is forced for a transect in the California current upwelling system on the west coast of Vancouver Island (VI transect) with wind forcing, and radiative forcing from the same region (Table 3.1).

Table 3.1: Data sets used to force the physical model. For the base run, wind and radiative forcing were taken from the year 1993. Other runs were performed using wind and radiative forcing from 2004 and 2008, and using alternative bathymetry with either a wider or narrower shelf width.

Forcing	Model
Bathymetry	Idealized (shelf width 40km, shelf depth 100m)
Wind Forcing	Meteorological buoy 46206 hourly wind data (48.83°N, 126°W)
Radiative Forcing	NCEP reanalysis (1.9°x2.4° region centred on 48.57°N, 125.62°W)
Buoyancy flux	None

Resolution Spatial resolution in the physical model is high. In the cross shore dimension, boxes are 0.953 km wide and the model domain extends 185 km offshore, which is well away from the 40 km wide shelf. I analyse model output within the first 90 km to focus on the effects of coastal upwelling and to avoid the offshore boundary. In the alongshore dimension, boxes are 1.67 km wide and the model domain is 5 km across. The vertical dimension is divided into 30 vertical sigma levels with a maximum box height of 186 m and a minimum box height of 1.61 m. Since the bathymetry is not a constant depth, the vertical boxes are taller further offshore. The vertical resolution is also adjusted so that it is higher at the surface and the base of the water column. Therefore the shallowest boxes are found directly onshore at the surface, while the deepest boxes are found offshore past the slope, and in the middle of the water column.

Bathymetry The original bathymetry (Bianucci et al., 2011) is based on a transect across the southern Vancouver Island shelf extending northeast to southwest from 49.00° N, 125.43° W to 48.29° N, 126.43° W. I altered this bathymetry slightly; my shelf is flatter and does not get as shallow at the coast as the original. The width of the shelf remains about 40 km (Figure 3.1).

The original bathymetry was modelled using a three part function. However, without wind forcing there was a slight irregularity in several variables at the crossover location of the transition between the functions. The spike was seen most obviously as a temporary increase in alkalinity in the water column above the transition from the shelf function to the slope function, and again at the transition from the slope function to the ocean bottom function. The new bathymetry is modelled using a single hyperbolic tangent function, which avoids irregularities since it is continuous, with a minimum depth of 98.7 m and a maximum depth of 1522 m.

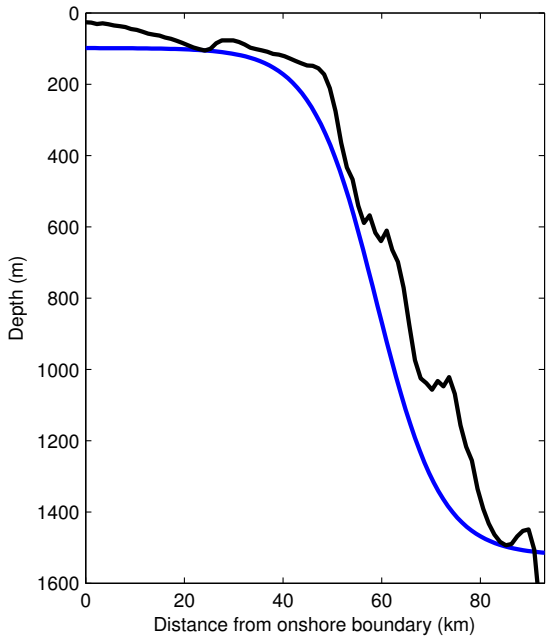

Figure 3.1: Model bathymetry approximated by a hyperbolic tangent (solid blue line). The model ocean bottom extends for another 100 km (not shown) in a nearly horizontal line. Bathymetry on the VI transect is shown in black (Foreman et al. 2008).

Initialization The model runs for 125 days over much of the upwelling season, beginning May 27th. Initialization values for the model are taken from observations along the southwest VI transect, with most modelled quantities (all but phytoplankton, zooplankton, ammonium, detritus, and argon) starting the run as the average of all available summer deep ocean profiles (variable with depth) and with all velocities beginning at zero. Initialization values are horizontally uniform in the along-shore and cross-shore dimensions but vary with depth. The offshore boundary uses a modified version of Orlanski's radiation open boundary condition (Raymond and Kuo, 1984).

Sensitivity Since my project is concerned with oxygen and argon in the mixed layer, I performed sensitivity runs using 0 mmol m^{-3} as the initial concentration for oxygen and argon in the mixed layer. Within 20 days, oxygen and argon had reached around 80% of concentrations in the mixed layer; therefore, I consider 20 days to be the spinup time. The weighting of the gas transfer velocity used to calculated

bioflux accounts for past variability in gas fluxes affecting current $\Delta O_2/Ar$, so the weighting and spin-up times should not overlap. Hence I analyze data after 50 days (20 day spinup followed by 30 day weighting) (Appendix A). Thus my model runs begin spinup on May 27th, weighting on June 16th, and the data used in analysis is from July 18th until September 29th for all years of forcing.

Wind stress and radiative forcing Wind stress is calculated from hourly wind data from meteorological buoy 46206 from May 27th to September 29th in 1993, 2004 and 2008 using the method of Smith (1988). The wind-stress is then filtered with a 6 hour low-pass Fast Fourier Transform filter. Heat fluxes from the same years are derived from NCEP reanalysis (Table 3.1). The forcing data used for the base run are from the summer of 1993, which is an average year for the region in terms of upwelling favourable winds (Bianucci, 2010).

The Vancouver Island coastal current The VI transect has unique oceanographic conditions within the California coastal current system (Freeland et al., 1984; Hickey and Banas, 2008). For example, the Vancouver Island Coastal Current (VICC), a northward flowing buoyancy current of low salinity water mainly from the Fraser river (Freeland et al., 1984), flows northward along the west coast of VI. It affects the area landward of the 100 m isobath and is between 15 and 25 km wide with maximum velocities typically around 10 cm s^{-1} (Hickey et al., 1991; Thomson et al., 1989). The VICC is a major source of nutrient rich, salinity poor water, which drives high primary productivity and masks the upwelling signal (Crawford and Dewey, 1989; Hickey and Banas, 2008). I excluded the VICC from this particular model to better examine the effects of upwelling on oxygen/argon ratios in coastal upwelling zones in general, rather than specifically on the VI transect.

3.1.2 Biological Model

The nitrogen based biological model is a modified version of Fennel et al. (2006) with an inorganic carbon component (Fennel et al., 2009, 2008). The main changes to this model are described in Bianucci et al. (2011) and involve dissolved organic carbon (DOC) cycling and sediment layer oxidization.

State variables The biological state variables, or modelled quantities, are phytoplankton (P - diatoms), zooplankton (Z - mesozooplankton), nitrogen and carbon

detritus (D_C and D_N), semilabile dissolved organic nitrogen and carbon (DOC_{SL} and DON_{SL}), nitrate (NO_3), ammonium (NH_4), dissolved inorganic carbon (DIC), total alkalininty (A), and oxygen(O_2). Oxygen is coupled to the carbon cycle rather than the nitrogen cycle since the model has an excess DIC uptake ($ExcessC$) when light is abundant but nitrogen (NO_3 and NH_4) is limiting (Ianson and Allen, 2002). This flux causes consumption of carbon and production of oxygen not associated with nitrogen. Carbon and oxygen are linked by photosynthetic quotients (PQ), number of moles of O_2 produced per mole of carbon dioxide assimilated. The PQ of nitrate based production is 1.4 (PQn), while the PQ of ammonium based production is 1.1 (PQa)(Laws, 1991).

Initialization and sensitivity Biological data are relatively rare, so modelled quantities were initialized as a small vertically uniform value (phytoplankton = 0.01 mmol m^{-3}, zooplankton = 0.01 mmol m^{-3}, ammonium = 0.01 mmol m^{-3}, and detritus = 0.1 mmol m^{-3}). Sensitivity analyses in which these initial conditions were varied by an order of magnitude of expected values were performed by Bianucci et al. (2011), who determined that results for these small vertically uniform values are independent of initial conditions after 50 days. I use a shorter residence time (20 days) given the more extreme sensitivity test used in this study (initialization of oxygen and argon as zero) (Appendix A).

Net community productivity

Net community productivity of oxygen (NCP) is defined as the sum of all the biological fluxes that affect oxygen in the biological model. The equation for NCP as taken from the model is:

$$\begin{aligned} NCP =& PQn(v^* f_I L_{NO_3} PR_{C:N}) + PQa(v^* f_I L_{NH_4} PR_{C:N} + \sigma_c ExcessC) \\ & - PQa\left(R_{C:N}\left[\omega_c P + (1-\beta)Q(1-\delta_c)gZ + \left(l_{BM} + l_E\beta\frac{g}{g_{max}}\right)Z\right]\right. \\ & \left. - f_{ox}(r_{DOC}DOC_{SL} + r_{D_C}D_C)\right) - n_{Nit}NH_4R_{C:N}(PQn - PQa) \end{aligned} \tag{3.1}$$

where $v*$ is the phytoplankton temperature dependant growth rate, f_I represents light limitation, L_{NO_3} and L_{NH_4} are nutrient limitation terms for NO_3 and NH_4 respectively, $R_{C:N}$ is the ratio of carbon to nitrogen, σ_C is the fraction of $ExcessC$ that

becomes DOC_{SL}, ω_C is the exudation rate of DOC_{Lab} (labile dissolved organic carbon), β represents the fraction of P grazed that is assimilated by Z, Q represents the fraction of unassimilated ingestion of P released as DOM, δ_C represents the fraction of DON_{SL} to total DON, g represents grazing of P by Z, l_{BM} represents a linear rate of basal metabolism for Z, l_E represents a maximum excretion rate for Z, g_{max} is the maximum grazing rate, f_{ox} describes the O_2 dependence of nitrification, r_{DOC} and r_{D_C} are rates of remineralization, and n_{Nit} is the rate of nitrification (Bianucci, 2010).

The source terms for NCP include new production, regenerated production, and excess carbon uptake (defined above). New production refers to nitrate-based production, while regenerated production refers to ammonia-based production.

Sink terms for NCP include phytoplankton exudation to labile dissolved organic matter (DOM) - which is immediately remineralized, nitrification, zooplankton grazing loss to dissolved inorganic carbon (DIC), zooplankton excretion and metabolism, carbon detritus remineralization, and dissolved organic carbon (DOC) remineralization.

Gas exchange

The gases involved in this project are oxygen, argon, and carbon dioxide. Argon was added as a physical tracer to this version of the model. It is initialized at equilibrium concentration based on initial salinity and temperature (Hamme and Emerson, 2004). Initial oxygen and carbon dioxide values were based on the average of all summer profiles available for the transect, and horizontally uniform (Bianucci et al., 2011). Gas exchange at the surface is calculated as

$$F_{x_{sea-to-air}} = k_X \cdot ([X]_{surf} - [X]_{eq}) \tag{3.2}$$

where $F_{x_{sea-to-air}}$ is the flux of gas X from the sea to the air, $[X]_{surf}$ is the concentration of the dissolved gas at the surface, $[X]_{eq}$ is the concentration of the gas at equilibrium based on salinity and temperature, and the gas transfer velocity, k_X, is calculated from Ho et al. (2006):

$$k_X = 0.266 \cdot U_{10}^2 \cdot \left(\frac{600}{Sc_X}\right)^{\frac{1}{2}} \tag{3.3}$$

where Sc_X is the Schmidt number for gas X, and U_{10} is the wind speed at 10 m.

Note that bubble-mediated gas exchange is not explicitly included nor is the effect of changing atmospheric pressure on $[X]_{eq}$. The Schmidt numbers for oxygen, argon, and carbon dioxide are calculated from Wanninkhof (1992). The equilibrium concentrations of the gases were calculated from Garcia and Gordon (1992, 1993) for oxygen, from Hamme and Emerson (2004) for argon, and from Weiss (1974) for carbon dioxide.

Drag coefficient The drag coefficient is needed to convert the wind stress forcing to wind speed for gas transfer velocity calculations. The model was altered to use a variable drag coefficient (Smith, 1988):

$$C_D = [K/ln(z/z_o)]^2 \tag{3.4}$$

$$z_o = au_*^2/g + 0.11v/u_* \tag{3.5}$$

$$u_* = \sqrt{\tau/\rho} \tag{3.6}$$

where C_D is the drag coefficient, z is height above the water (10 m), z_o is roughness length, τ is wind stress at the sea surface, ρ is the density of air, K is the von Karman constant (0.4), a is the Charnock constant (0.011), g is the acceleration due to gravity ($9.8ms^{-2}$), v is the dynamic viscosity for air ($14 \times 10^{-6}m^2s^{-1}$), and u_* is the friction velocity ($a = 0.018$ is suggested for coastal areas, however the wind forcing files were converted from windspeeds using $a = 0.011$ and so for the sake of consistency, that is the value used).

3.2 Model output analysis

The parameters of interest in my problem that are not directly calculated by the model are mixed layer depth (MLD), the biological sea-to-air flux of oxygen (bioflux), and other fluxes integrated over the mixed layer (rate terms and entrainment). I calculated these quantities from model output as follows:

3.2.1 Mixed layer depth and surface resolution

I defined the mixed layer depth used in data analysis as the depth at which the change in density from the surface was greater than 0.125 kg m^{-2} (Thomson and Fine, 2003). The Bianucci et al. (2011) setup of the model had little resolution in the

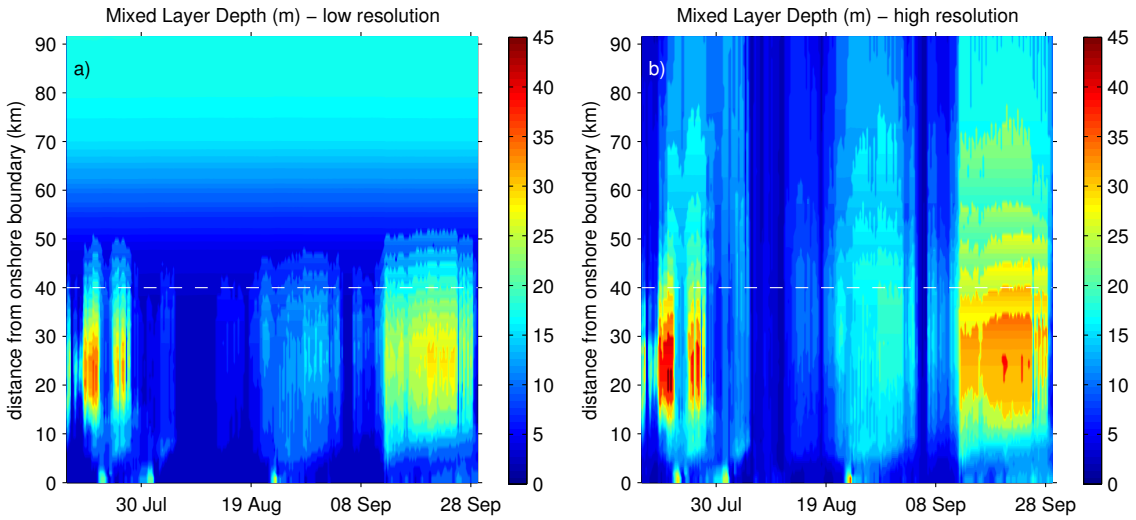

Figure 3.2: Distance from the coast on the y-axis vs time of year in the run on the x-axis. The first 50 days of the run (the combined spinup time and weighting time) are not shown - the plot starts July 18th. a) Mixed layer depth with low resolution of vertical layers at the surface, and b) mixed layer depth with high resolution of vertical layers at the surface. White line represents location of the shelf break. Wind forcing for these model runs is shown in Figure 5.1e.

surface ocean, especially off the shelf where the water column is significantly deeper. For example, the boxes at the surface were 16 m deep, creating a large vertical gradient and unrealistic mixing fluxes in the mixed layer in several variables such as temperature, salinity, and oxygen. The large salinity and temperature gradient in turn confined the mixed layer almost exclusively to the first box. Therefore, I increased the resolution of the vertical boxes at the surface (specifically the variable $theta_s$ in the input file was changed from 3.0 to 10.0). The new resolution resulted in a maximum surface box depth of 2.06 m, and a maximum box depth in the mixed layer of 8.8 m, which gave a much more reasonable gradient and allowed the mixed layer depth offshore to vary over the course of the run (Figure 3.2).

3.2.2 Calculation of the sea-to-air flux of biological oxygen using O_2/Ar

Gas exchange was calculated offline exactly as in the model (section 3.1.2). Bioflux was calculated from model oxygen (O_2) and argon (Ar) concentrations (section 2.1), wind speed (section 3.1.2 - drag coefficient), and mixed layer depth (section 3.2.1).

3.2.3 Gas transfer velocity weighting

Gas transfer velocity is weighted as described in section 2.2. I apply the weighting scheme for 720 hourly timepoints, equivalent to 30 days. The original Reuer method as described in section 2.3 uses 60 days, but there is little difference between bioflux weighted over 60 days and bioflux weighted over 30 days (section 5.2 - Weighting times in the calculation of k_{O_2}). A weighting period of 30 days is also more appropriate given that coastal upwelling zones tend to be much more dynamic than the open ocean. Wind forcing is consistent over the entire model domain at any given time, although the gas transfer velocity is not consistent due to dependance on the Schmidt number, which depends on surface temperature and varies in space along the model transect.

3.2.4 Rate terms and entrainment

The model records data every 6 hours, although the actual timestep is adaptive and much shorter. Net rates of advection and diffusion of oxygen and argon into each box, time averaged over 6 hours, as well as the rate of change term which represents the $\delta/\delta t$ term are available. Horizontal diffusion of tracers is uniformly equal to zero in the model so I do not consider this flux further. I integrated these fluxes over the boxes in the mixed layer depth at each time point to examine the mass balance of biological oxygen in the mixed layer :

$$\sum \frac{\delta bioO_2}{\delta t} = \sum NCP - k_{O_2} \cdot \Delta O_2/Ar \cdot [O_2]_{eq} + \sum F_{vdiff\_bioO_2} + \sum F_{vadv\_bioO_2} + \sum F_{hadv\_bioO_2} \tag{3.7}$$

where F represents the various biological fluxes (vertical diffusion, vertical advection, horizontal advection). $\delta bioO_2/\delta t$ represents the rate of change term. Since the model calculates the rate of change terms as the sum of these fluxes, this equation is exact as long as integration times are sufficiently short. Similar to the calculation of bioflux, argon fluxes are used in order to transform physical oxygen fluxes output by the model to fluxes of biological oxygen (Giesbrecht et al., 2012).

$$F_{biologicalO_2} = F_{O_2} - (F_{Ar} \cdot [O_2]_{eq}/[Ar]_{eq}) \tag{3.8}$$

where F_{O_2} represents the flux of oxygen as output by the model, F_{Ar} represents the flux of argon as output by the model, and $[O_2]_{eq}/[Ar]_{eq}$ represents the ratio of oxygen equilibrium concentration over argon equilibrium concentration.

An entrainment term was also calculated offline to estimate total biological oxygen either added to, or removed from, the mixed layer due to a change in mixed layer depth:

$$entrainment = \left(\frac{\delta z}{\delta t} \cdot \Delta O_2/Ar \cdot [O_2]_{eq}\right) \tag{3.9}$$

where z is depth increasing downwards, $\frac{\delta z}{\delta t}$ represents the change in mixed layer depth since the last timestep (positive for entrainment, and negative for detrainment), $\Delta O_2/Ar$ represents the biological supersaturation of oxygen in the boxes added to or removed from the mixed layer, and $[O_2]_{eq}$ represents the equilibrium concentration of oxygen based on salinity and temperature at the timestep before entrainment.

Entrainment occurs implicitly in the model mainly via vertical diffusion. For example, suppose biological oxygen was supersaturated underneath the mixed layer and a storm began. As mechanical energy supplied by the winds increases, vertical diffusion increases and causes a flux of biological oxygen from the boxes below the mixed layer into the boxes within the mixed layer. Model quantities become more homogeneous over a greater depth, and the mixed layer deepens. The vertical diffusion term in my mass balance includea the flux of biological oxygen from the boxes entering the mixed layer to the boxes in the formerly shallower mixed layer. The increase in biological oxygen in the upper boxes is also included in the $\frac{\delta bioO_2}{\delta t}$ term (left hand side of equation 3.7). However, none of the terms in my mass balance accounts for the biological oxygen which remains in the boxes that have been added to the mixed layer. This explicit entrainment term (Equation 3.9) is not part of the mass balance since it would count the entrained oxygen within the vertical diffusion term twice, but I present the term for comparison to the other mass balance terms.

Chapter 4

Model Validation

This project focusses on gas exchange at the ocean surface as it relates to net community productivity, so both gas ratios and saturations in the mixed layer, along with realistic portrayal of mixed layer dynamics are critical. I compared observations on and near the VI transect with model data for $\Delta O_2/Ar$ distribution and argon saturation. In addition, I looked at mixed layer depths from the model and from the VI transect as they relate to wind forcing and gas exchange.

4.1 $\Delta O_2/Ar$ distribution

Observed distributions of $\Delta O_2/Ar$ values from (or near) the VI transect (between 48°N - 51°N and 124°W - 129°W) in late May of 2007 and 2010 (Tortell et al., 2012) were compared to the distribution in the base model run (Figure 4.1). The observations were collected approximately every 0.33 km - slightly higher resolution than the model, while underway, at the surface of the ocean (4.5 m depth, collected at the bow of the ship in order to prevent mixing due to the passage of the ship). Model data are taken from the mixed layer on a 92 km transect sampled every 6 hours over 75 days. The average MLD during this time period is 13.1 m with a maximum of 46.8 m and a minimum of 1.8 m.

The model run yields significantly more data ($n_{model} = 28906$) than the observations ($n_{2007} = 3250$, $n_{2010} = 6541$) and covers a later time period following spring, but the distribution appears similar to the VI data, with the peak of all distributions occurring between 2-3% (Figure 4.1). The data fall off sharply near 0% especially in the model and in the 2007 observations although negative values are present in

all three records. The model data include more highly negative values; however, the cruise data were collected over a shorter period of time with no major upwelling favourable wind events (associated with negative $\Delta O_2/Ar$) occurring during data collection (Tortell et al., 2012). Both VI cruises collected some data within the VICC but these data fall within the overall distribution. Most importantly, the model distribution includes most of the observations from the VI region. Most of the data fall between 1 and 15% in all three distributions. In 2007 there are mostly positive data, with supersaturations reaching up to 40%. In 2010 values are generally lower, and there are some negative data. The model data span both of these distributions, although the rare, exceptionally high (40%) values are not achieved in the model base run. In addition, the higher proportion of small positive $\Delta O_2/Ar$ seen in the model data can be attributed to much of the observational data being collected near shore where values tend to be more extreme (Tortell et al., 2012). Therefore, while 2007 and 2010 were quite different years, both are similar to the longer, highly sampled, model record in regards to $\Delta O_2/Ar$ distributions.

4.2 Argon supersaturation

I added argon during the course of this project and assigned initial values and boundary conditions based on equilibrium concentrations. Argon data are rare. To ensure that this equilibrium assumption was reasonable, water samples from August 2013 were collected (Appendix B) and compared to model data (Figure 4.2a). The data plotted are an average of two replicates (pooled standard deviation = 0.12%) taken at a water column depth of 114 m and 1300 m, which correspond to 30 km and 70 km offshore in the model, respectively. Three of these five discrete observations fell within the ranges of values found in the model over the course of a month (Table 4.1).

The shelf datum at 30 m depth is the observation that is the farthest out of the modelled range of Ar supersaturations (Table 4.1). The maximum in Ar supersaturation at 20-25 m in the model is likely caused by subsurface heating. When water below the mixed layer is warmed, its concentration is not affected, but its solubility decreases, causing the supersaturation to rise. It could be that the surface heating that penetrates below the mixed layer in the model is distributed more deeply than the region where the measurements were made. The model would only have to have increased temperature by 0.5°C in order to change the argon supersaturation by slightly more than 1%.

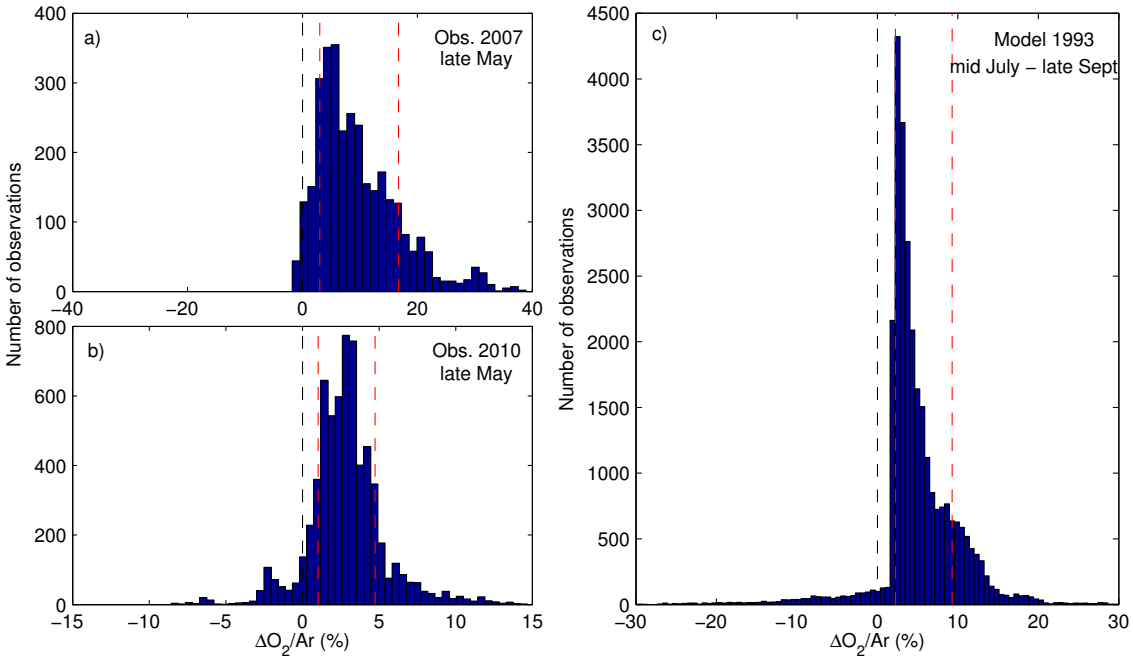

Figure 4.1: Distribution of surface $\Delta O_2/Ar$ values from the west coast of Vancouver Island in 2007 (a) and 2010 (b) and from the base model run (c). The data from the cruises are from late May of their respective years (Tortell et al., 2012) while the model data from the base model run span late July until late September. Note that the x-axes have different limits. Black dashed lines represent 0. 70% of the data are contained between the red dashed lines of each distribution. Distributions from model runs forced with 2004 and 2008 form the same shape (Appendix D).

The on-shelf point at the base of the water column that does not fall within the range of model data is less than 1% out of the modelled range of supersaturation, meaning that temperatures near the bottom would only need to have decreased by 0.3°C to achieve the higher value that is observed. Regardless, the point is near the base of the water column while the focus of this thesis is on processes near the ocean surface. In general, the observed argon supersaturations fall within the range predicted by the model. The points where supersaturations fall outside of this range can be explained by the model temperature either slightly increasing or slightly decreasing.

Table 4.1: Discrete observations compared with mean and extreme model argon saturations. Argon observations in the VI region were made from August 22 - August 23, 2013 (Appendix B). Model data over a full month centred around the year day of observations are considered.

Depth (m)	Water column depth (m)	Measured Δ Ar (%)	Mean model Δ Ar (%)	Max model Δ Ar (%)	Min model Δ Ar (%)
29.8	114	1.97±0.01	3.63	3.90	3.21
49.4	114	1.22±0.07	1.40	1.67	1.18
99.2	114	0.72±0.09	0.02	0.06	-0.02
30.1	1300	3.24±0.03	2.88	3.22	2.50
99.6	1300	0.51±0.12	0.18	0.42	0.01

4.3 Gas transfer velocity vs mixed layer depth

Mixed layer depth dynamics are important as this project is concerned with measuring biological fluxes within the mixed layer. The observed mixed layer depths were estimated (as in the model, section 3.2.1) from conductivity-temperature-depth casts (D. Yelland, pers. com.) collected in the region (48-49°N, 125-127°W) outside the VICC during regular monitoring by Fisheries and Oceans Canada during my three model years (e.g. Mackas, 1992; Tortell et al., 2012). These data were then compared to model mixed layer depths (section 3.2.1) and associated wind forcing at that point in time. The weighted gas transfer velocity for oxygen was calculated from wind speed from the same period of time (section 2.2) using forcing winds from the model. I compare mixed layer depth plotted against weighted gas transfer velocity (Equation 2.4-2.6) for model data ($n_{model} = 144627$) and the observations ($n_{obs} = 57$)(Figure 4.2 b).

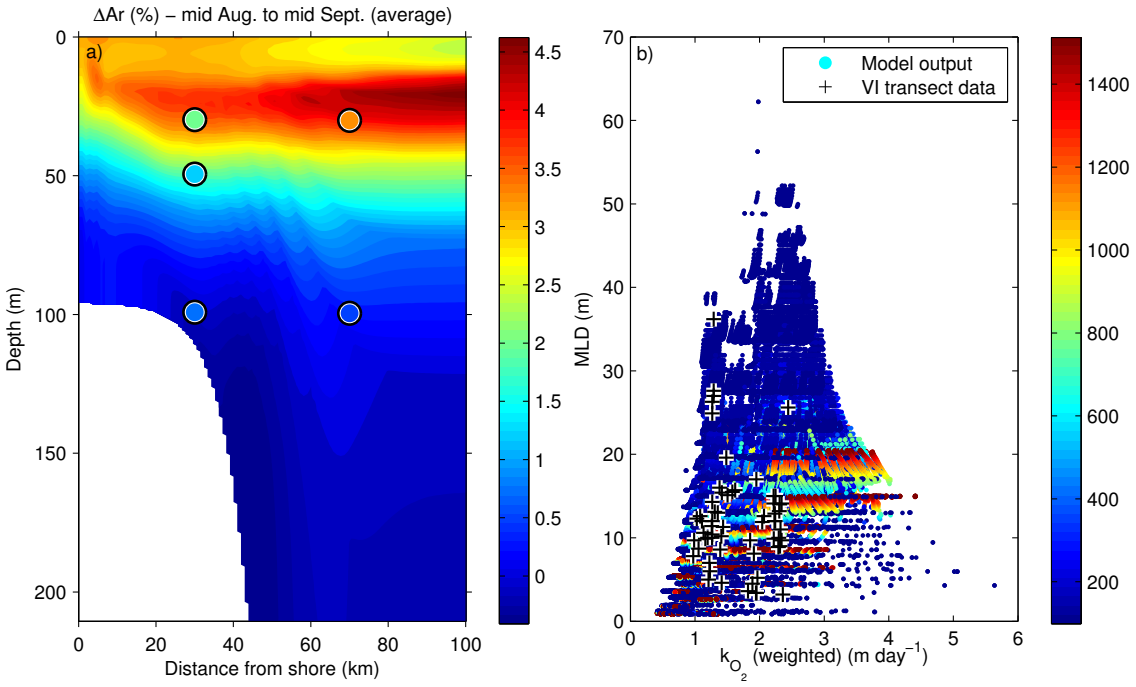

Figure 4.2: a) Mean model argon supersaturation in the mixed layer from mid-August to mid-September with discrete argon measurements (circles) collected near the VI transect at 114 and 1300 m column depth in August 2013. b) Mixed layer depth vs weighted oxygen gas transfer velocity (section 2.2) from the base run and the 2004 and 2008 runs of the model (points colour coded by water column depth) and from observations (black crosses) from several years of data near the transect (excluding the first 20 km from the coast) (June 26-28 1993, May 26-28 2004 and 22-24 2008, September 8-9 2004 and 1-8 2008).

The observations fall well within the range of values that occur in the model, although there are no data at higher values of weighted gas transfer velocity. Few data are available during strong wind forcing, which leads to a bias in observations toward low gas transfer velocities. In addition, the deeper mixed layer depths coincide with the nearshore portion of the shelf where upwelling occurs in the model. (Data from this region were excluded from the observations due to the presence of the VICC.) The observations were not able to capture any upwelling events, which are sporadic so I do not expect mixed layers at the deep end of the model range. 75% of all MLDs in the model are less than 17 m deep, while in VI transect data, 75% are less than 15 m deep. The average mixed layer depth for both model and VI transect data is 12 m. Thus the model represents mixed layer depths and dynamics accurately.

Chapter 5

Results and Discussion

5.1 General model results

The model domain in this project represents a coastal upwelling zone. It is used to explore whether NCP can be estimated from oxygen/argon ratios despite violations of key assumptions, in particular steady state. In such regions, upwelling is driven by prevailing equatorward winds along the coast, and during the summer, these winds are common. Upwelling brings subsurface water (low in oxygen, high in carbon and nutrients) from intermediate depths to the surface (Smith, 1994).

Wind forcing Over the course of the base run (1993), winds are most often upwelling favourable but not particularly strong. There are a couple of strong downwelling events, the strongest in late August, and one strong upwelling event in mid September (Figure 5.1e).

Physical The effects of upwelling and downwelling are clearly seen in salinity, with saltier water added to the mixed layer during upwelling favourable winds, and less salty water being drawn back towards the shore during downwelling events (Figure 5.1a). Argon saturation in the model starts at equilibrium everywhere. Therefore argon increases with depth as temperature decreases, so upwelling events are associated with higher argon concentrations. As with salinity, the physical effects of upwelling and downwelling on argon concentrations (Figure 5.1b) are more clear than they are with the biological variables. Higher concentrations of argon are brought to the surface during upwelling favourable wind events, most noticeably during the strong event in mid September. Gas exchange causes these higher concentrations

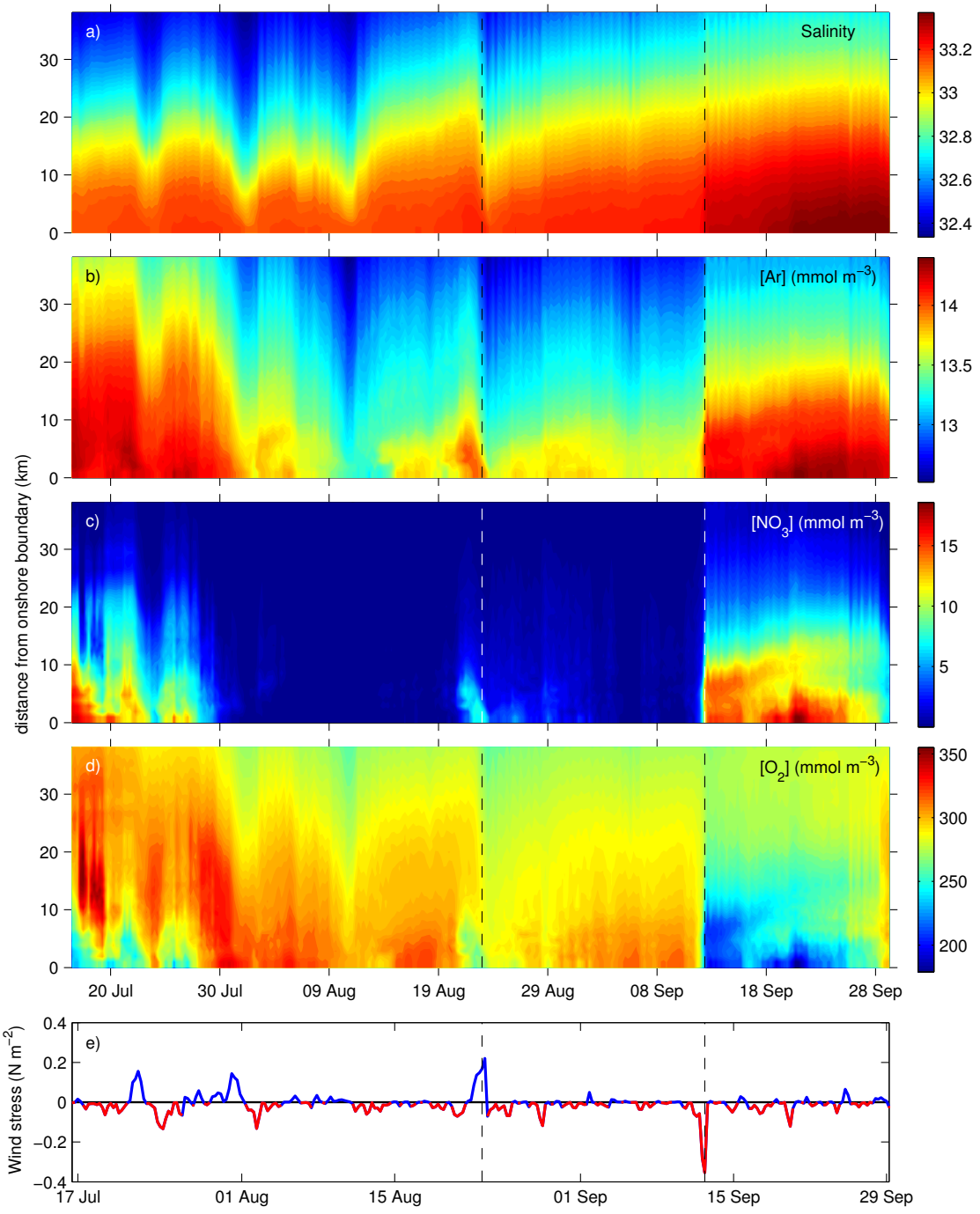

Figure 5.1: Average a) salinity, b) argon, c) nitrate, and d) oxygen in the mixed layer over the shelf - the inner 40 km of the model domain - distance offshore vs. time, and e) associated alongshore wind forcing (wind forcing vs. time), uniform over the model domain for the base run (1993). Negative wind forcing (red) is associated with upwelling, while positive wind forcing (blue) is associated with downwelling. Dashed lines represent two points of interest - from left to right, a major downwelling event (late August) and a major upwelling event (mid September).

along the shore to decrease faster with time than salinity; specifically, near the end of July and moving into the beginning of August, nearshore salinity is maintained at a higher level, while argon concentrations are driven back towards equilibrium. During downwelling favourable winds, the higher argon concentrations retreat onshore (e.g. late August)(Figure 5.1b).

Biological During times of upwelling favourable winds (red, Figure 5.1e), there is an influx of low oxygen, and high nitrate water to the mixed layer near the shore (Figure 5.1c,d). A large upwelling event occurs right before the beginning of the period of time being analyzed, which is why the concentration of oxygen is low and nitrate high at the beginning of the displayed run. Similar, although opposite, patterns can be seen in oxygen and nitrate since they are both involved in photosynthesis. As high nitrate water is added to the mixed layer, phytoplankton take it up fueling biological production of oxygen. Over time, oxygen decreases overall in the mixed layer due to warming in the model domain, which decreases the equilibrium saturation, thereby decreasing outgassing.

5.2 Temporally and spatially averaged NCP

NCP in the mixed layer and bioflux (Equation 2.3) at the surface are largely a product of the wind forcing (Figure 5.2a,b). At times when there is upwelling favourable wind forcing (most notably around mid September), there is a large influx of oxygen into the mixed layer (displayed as negative bioflux, Figure 5.2a) at the surface due to the upwelling of water undersaturated in oxygen. At the same time, NCP increases quickly as a result of the influx of nutrients to the mixed layer. Even at locations slightly offshore or just after an upwelling event where positive bioflux is observed, bioflux is rarely an accurate estimation of instantaneous NCP due to the bioflux lag effect (section 2.3).

Because this lag (the time necessary to ventilate the biological oxygen) is significant, I averaged NCP over the residence time of oxygen with respect to gas exchange in the mixed layer (section 2.3). Mean residence time due to gas exchange in the mixed layer averaged over the model domain in space and time is 9 days based on the weighted gas transfer velocity. The maximum residence time is 38 days, which is therefore the maximum amount of time that it should take to ventilate 63% of the biological oxygen in the mixed layer to the atmosphere if wind and mixed layer depth

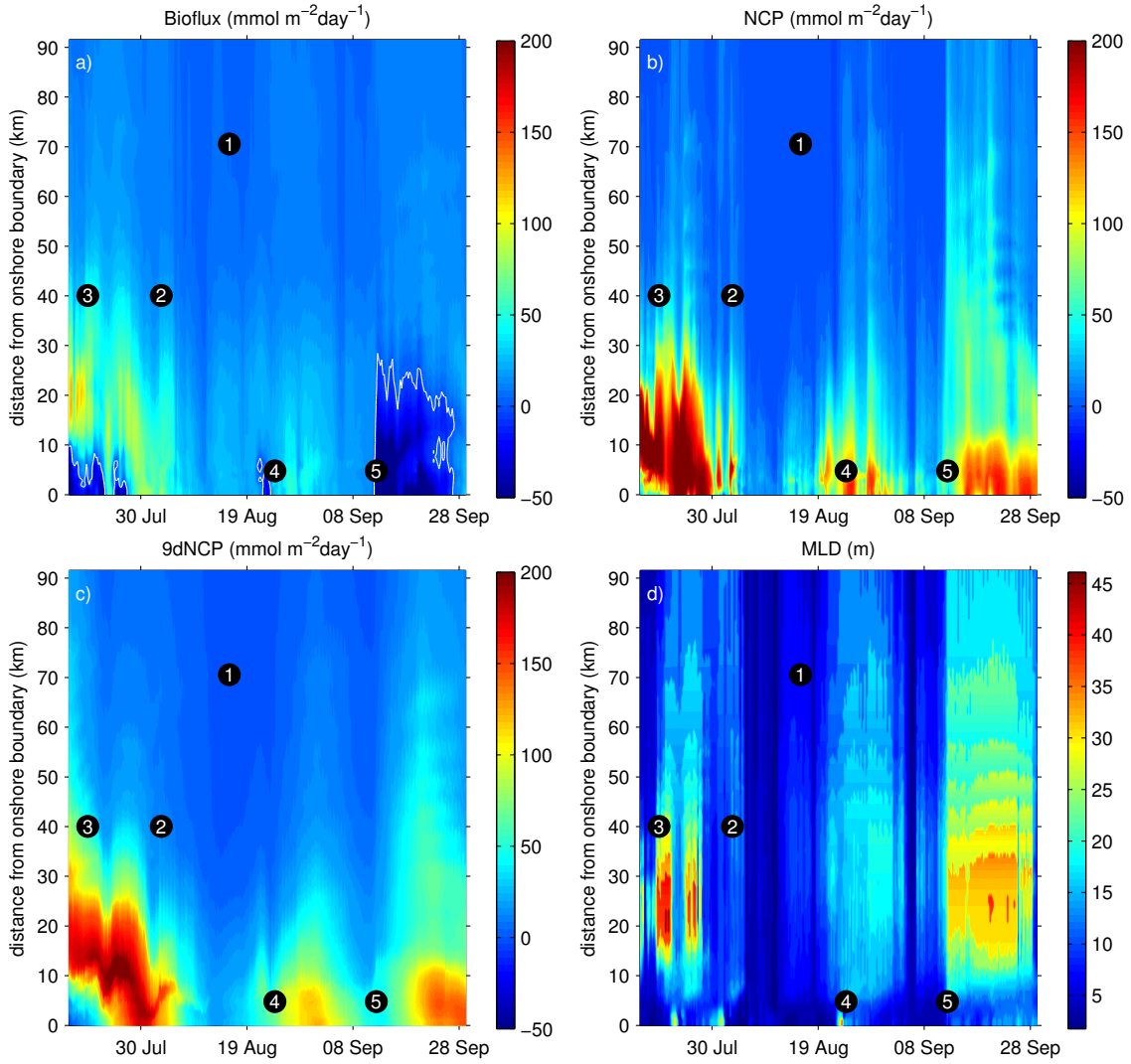

Figure 5.2: Property plots within 90 km of the shore over the course of the base run (1993). a) Bioflux (white contours represent the division between positive and negative values), b) instantaneous mixed layer NCP, c) mixed layer NCP averaged (following the Lagrangian advection of the water parcel) over the previous 9 days, and d) mixed layer depth. Numbers refer to specific locations of interest discussed in section 5.3.

conditions remain stable. However, this length of residence time with respect to gas exchange is only seen at a couple of points throughout the run corresponding to low wind forcing and deep mixed layer depths, so true ventilation times are always shorter than this maximum value because the mixed layer shoals or wind forcing increases. If the residence time were calculated at every model time step (6 hours) using the instantaneous gas transfer velocity, the maximum residence time would be 7100 days, the minimum 0.80 days, and the average residence time would be 59 days (the median is 13 days). The average residence time based on instantaneous gas transfer velocities is heavily influenced by a few outlier values corresponding to very low wind speeds which cause long residence times. Since the mean residence time with respect to weighted gas exchange is just under 9 days, I decided to compensate for the lag effect by using a 9 day average NCP to compare to bioflux. To link this averaging time to observations taken in the field, a wind record and a current mixed layer depth can be used in order to estimate the residence time with respect to gas exchange. This estimate indicates the time-scale for the measurement of bioflux.

Horizontal Advection To account for advection in the model, NCP was averaged both temporally and spatially following the Lagrangian path of the water (Figure 5.2c). For a given point in time and space, the horizontal distance and direction that the contents of that box moved in the past 6 hour timestep were calculated from the horizontal velocity associated with that box. Then the NCP for the box corresponding to the location one timestep ago was added to the instantaneous NCP for the current box (Figure 5.3a). This process was repeated, using a 6 hour timestep over 9 days, after which the averaged NCP was calculated from the sum. Figure 5.3 illustrates the motion of specific parcels of water over 9 days. Inertial oscillations in advection are clear with a period of about 17 hours (Kundu and Thomson, 1990). Due to the setup of the model, the integration time is limited to a 6 hour timestep. To ensure this time step was sufficiently short, I performed the spatial and temporal averaging using a 12 hour timestep. Total NCP over the course of the model run was about the same (difference of less than 1%). In addition, the total NCP over the course of the run averaged temporally was compared with the total NCP averaged spatially and temporally. Again, the difference between the two was less than 1%. These two experiments demonstrate that mass is conserved when NCP is averaged temporally and spatially. In addition, Figure 5.3b displays the maximum distance offshore travelled over the course of 9 days, referring to the distance between the start

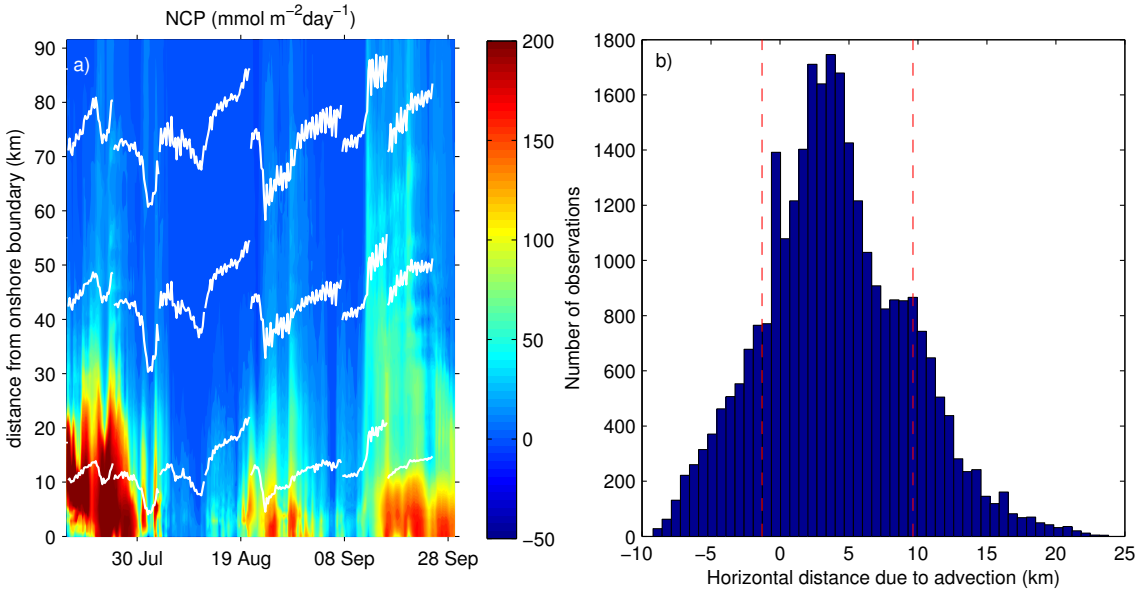

Figure 5.3: a) Instantaneous NCP with advection tracks showing the horizontal advection of the water in the mixed layer over 9 days beginning at either 10, 40, and 70 km offshore. Advection tracks begin every 9 days at each distance offshore. b) Distribution of the horizontal distance water parcels are advected over the course of 9 days. Distance refers to the net difference between the start and end point rather than the total distance travelled. 70% of the data are contained between the red dashed lines.

and end points rather than the total distance travelled. The horizontal advection in the base run creates an offset of 25 km at some points between the location at which biological oxygen is created, and the point at which most of it has been outgassed. This model does not simulate alongshore advection. In reality, the Lagrangian path will be both offshore and alongshore. Regardless, bioflux will still represent NCP along the Lagrangian path of the water parcel over the past 9 days.

Vertical advection The same calculation was performed including vertical advection; however, every parcel of water remained within the mixed layer over the course of 9 days. The mean rate of vertical advection in the mixed layer is 5x10^{-7} m s^{-1} (0.04 m day^{-1}). In the mixed layer, 85% of vertical advection values fall below 2x10^{-5} m s^{-1} (2 m d^{-1}), which, if vertical advection remained consistent at this value, will rarely carry the parcel out of the mixed layer. With mixed layer depths ranging from 1.8 m to 48.6 m and with higher advection values often short lived (usually one or two timesteps), nearly every parcel of water remains within the mixed layer over the

course of nine days. Therefore I calculate temporally and spatially averaged NCP considering only advection in the horizontal plane.

Temporally and spatially averaged NCP (Figure 5.2c) continues to show effects of photosynthetic blooms after the bloom itself has ended as shown by instantaneous NCP (Figure 5.2b). This averaging helps account for the bioflux lag (section 2.3) and accounts for some points in which bioflux is higher than instantaneous NCP.

Weighting times in the calculation of k_{O_2} Reuer et al. (2007) uses a gas transfer weighting time of 60 days, but I use a 30 day weighting to calculate the gas transfer velocity due to the dynamic nature of the coastal upwelling system. There is rarely a point in coastal upwelling zones where the wind conditions 60 days ago will have any effect on the current state of the mixed layer, because, due to a dynamic mixed layer, strong wind forcing, and significant advection and diffusion, the contents of the mixed layer have been refreshed. Over the course of 60 days, the weighting coefficent (ω_i - section 2.2) used to calculate the weighted gas transfer velocity for any given day decreases, ideally approaching zero by the end of the weighting period (Figure 5.4). Using 60 day weighting, 99.9% of the time in my base run of the model, the weighting coefficient values fall below 0.1 (10%) by the end of the weighting period. Using a 30 day weighting scheme, 92% of values fall below 0.1, and those that do not are mostly associated with the unusual time period at the end of the run where the gas transfer velocities are consistently low and the mixed layer is deep, leading to abnormally high residence times with respect to gas exchange as compared to the mean. Higher wind forcing corresponds in general with higher gas exchange coefficients and a rapid ventilation of the mixed layer, which reduces the weighting coefficient rapidly (Figure 5.4a,b, e.g. point 1). Conversely, slow ventilation times cause only a gradual reduction in the weighting coefficient.

Using a 30 day weighting time as opposed to a 60 day weighting time does not result in a significant change in bioflux values. The difference between the mean bioflux excluding the first 50 days using a 30 day weighting and using a 60 day weighting is 0.6 mmol $m^{-2}day^{-1}$, and the percent difference is 0.9% (When using the 60 day weighting for days 50-60, the 10 days previous to the beginning of the run are assumed to be identical to the initial conditions of the model)(Figure 5.5). Comparing bioflux values every 6 hours between the 30 and 60 day weighting schemes, 70% of the values are close, and have a percent difference falling between 6% and -3%.

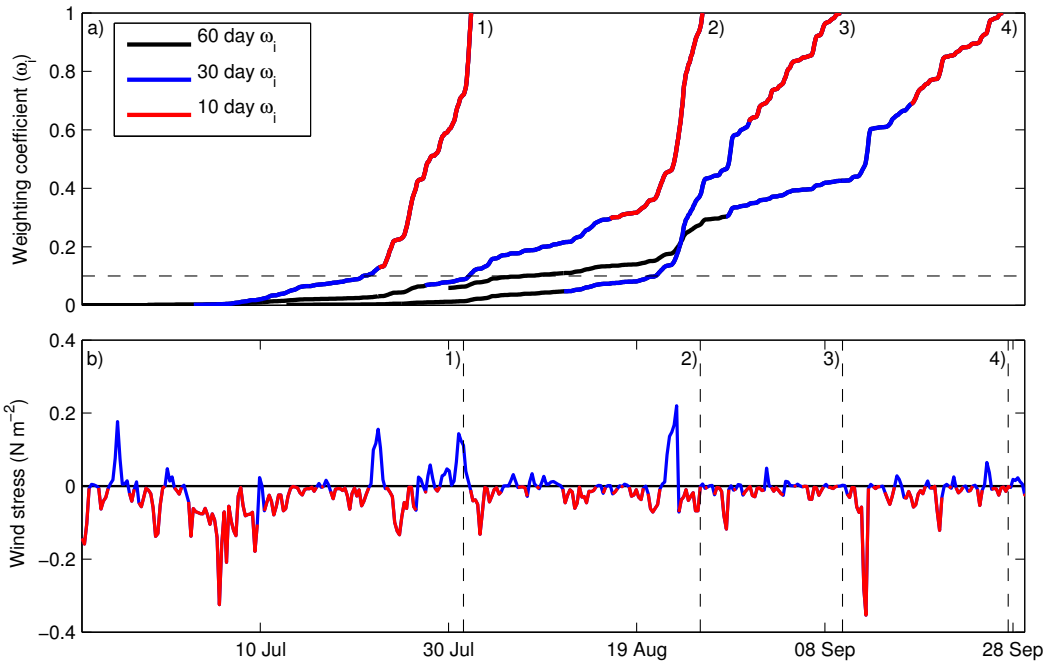

Figure 5.4: a) Examples of the decay with time of individual weighting coefficients on four specific days for the calculation of the weighted k_{O_2} over 60 (black), 30 (blue) and 10 (red) days. For the first 10 days, all three lines lie on top of each other, and for the subsequent 20 days, the blue and black lines lie on top of each other. b) Wind forcing from mid-June to late September. Black dashed lines represent the days for which corresponding weighting coefficients (as numbered) are displayed in panel a. The wind forcing is extended before the beginning of the analysis time (July 16th) to show 30 and 60 day weighting during that time period.

5.3 Accuracy of bioflux as a proxy for NCP

To demonstrate the effects of different environmental factors on the use of bioflux as a proxy for NCP, I will examine fluxes of oxygen in the mixed layer at several different locations and times in detail as indicated in Figure 5.2. I will consider instantaneous fluxes in the mixed layer at each of these points (Figure 5.6), and the cumulative fluxes over the course of the run at various distances offshore (Figure 5.7). The rate of change represents the $\delta/\delta t$ term, and the fluxes are as described in section 3.2.4. The entrainment term (Equation 3.8) is not included in the calculation of the rate of change term. Positive fluxes represent fluxes into the mixed layer, while negative fluxes represent fluxes out of the mixed layer (therefore while NCP is a positive flux, bioflux is usually a negative flux in these plots when it is a flux out of the mixed

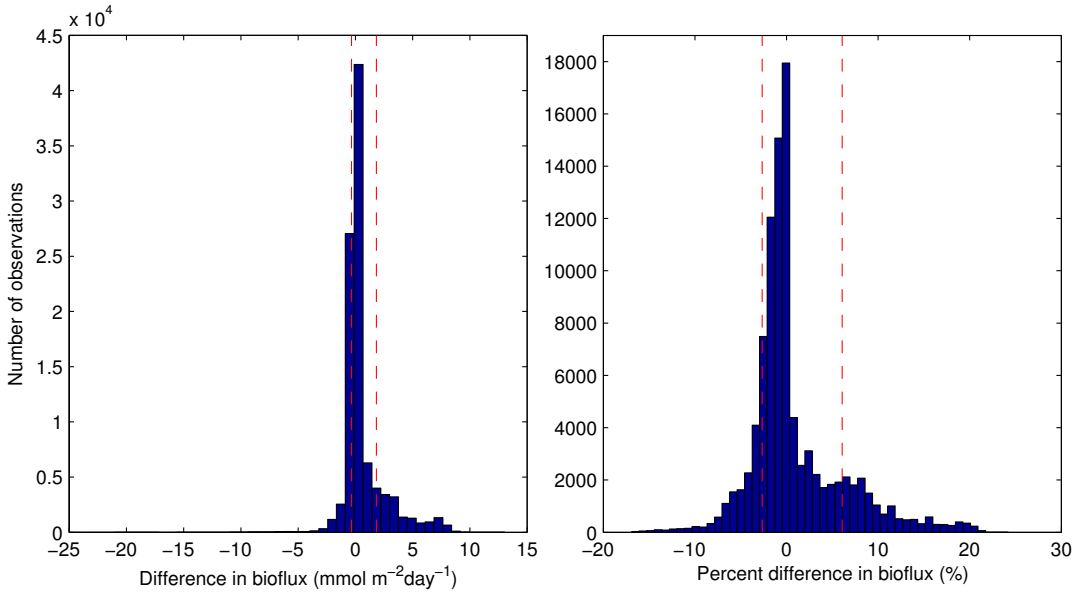

Figure 5.5: a) Difference between bioflux weighted using a 30 day weighting scheme and bioflux weighted using a 60 day weighting scheme. b) Percent difference between bioflux weighted using a 30 day weighting scheme and bioflux weighted using a 60 day weighting scheme. 70% of the data are contained between the red dashed lines of each distribution.

layer). I use the abbreviation 9dNCP to refer to NCP averaged spatially following a Lagrangian path over 9 days.

NCP and bioflux balanced (1) The first point I chose (mid-August, 70km offshore)(Figure 5.6) demonstrates a situation where bioflux is a fairly good proxy for both instantaneous NCP and 9dNCP, but all are low. Here, the level of instantaneous NCP has been fairly constant for at least the past 9 days and there is little advection, so the instantaneous and averaged NCP are similar. The mixed layer at this point has been constant for several days previous (10 m). Biological oxygen is higher beneath the mixed layer (Figure 5.7a), and a small positive vertical diffusion at the base of the mixed layer increases biological oxygen in the mixed layer ($\delta O_2/\delta t$ positive) (Figure 5.6). This flux contributes to the small overestimation of 9dNCP (which is confined to the mixed layer) by bioflux. At this location, oxygen concentrations are lower than mean values closer to shore. Over the course of the run, bioflux and NCP remain similar with the cumulative values mirroring each other throughout the run (Figure 5.7b).

Entrainment of high oxygen water (2) The second point I chose (early August, 40 km offshore, shelf break) (Figure 5.6) demonstrates a situation in which the mixed layer deepens and entrains the water directly below with high biological oxygen (Figure 5.7c). In this situation, much of the increase in oxygen in the mixed layer is caused by the deepening of the mixed layer as opposed to productivity within the mixed layer. Therefore bioflux includes productivity that occurred below the mixed layer. There is also high vertical diffusion at this point; e.g. entrained oxygen from the new model boxes in the mixed layer. Although this point represents a moment in which bioflux is a overestimate of mixed layer NCP, overall at this distance offshore, bioflux and NCP are broadly similar over the course of the run (Figure 5.7d).

Averaging accounting for bioflux lag (3) The third point (late July, 40 km offshore, shelf break) demonstrates the bioflux lag. Here bioflux is a good estimate of the 9 day spatial averaged NCP while the instantaneous NCP is much lower (Figure 5.6). There has been productivity occurring over the past 9 days (Figure 5.7c), therefore biologically produced oxygen that is present in the mixed layer is representative of NCP over the past 9 days. This point is on the outside edge of a bloom, where productivity has been decreasing, which is the reason for the lower instantaneous NCP value - an illustration of the bioflux lag effect (section 2.3). Also the advection and diffusion terms balance each other at this point and have little effect on the mass balance, which means that the biological oxygen leaving the box is almost exclusively through gas exchange, and that gas exchange is representative of the temporally and spatially averaged NCP.

Upwelling leading to bioflux out of the mixed layer (4) The fourth point (late August, 5 km offshore) is an example of bioflux underestimating NCP due to recent upwelling. This point occurs at the start of an upwelling favourable wind event. Bioflux is out of the mixed layer, but strongly affected (reduced) by the upwelling of water undersaturated in oxygen. All the physical fluxes in this situation are strongly negative (Figure 5.6; note the change in scale for this example (4)), so biological oxygen is lost from the mixed layer before it can be outgassed. The rate of change term is also negative which reinforces the fact that the concentration of oxygen is decreasing in the mixed layer due to upwelling and diffusion of undersaturated water. This far onshore, there is significantly more NCP over the course of the run (Figure 5.7f) as expected. The majority of the productivity happens where the water

that is high in nutrients is upwelled at the shore, but the nutrients are usually largely consumed by the time the upwelled water is advected offshore. The bioflux at this distance from shore tends to underestimate NCP over the entire run.(Figure 5.7f).

Upwelling leading to bioflux into the mixed layer (5) The fifth point (mid September, 5 km offshore) is an example of undersaturated waters at the surface causing bioflux into the ocean from the atmosphere. It occurs during an incredibly large upwelling favourable wind event which causes large instantaneous fluxes (Figure 5.6). Specifically, there is a lot of advection and diffusion out of the mixed layer, the diffusion being mainly due to the entrainment of oxygen poor water in to the mixed layer which causes a negative diffusion flux as oxygen diffuses downwards into the newly added boxes. At the same time, net advection is negative either due to upwelling of water undersaturated in biological oxygen, offshore advection of oxygen supersaturated in biological oxygen, or both. This combination of fluxes leads to net losses of oxygen and a lowering of oxygen saturation (change in oxygen with time term is negative) (Figure 5.6). Since the saturation of oxygen is so low, net productivity is not reflected in a calculation of bioflux. Because bioflux is into the mixed layer, this point would be discounted based on current practices in the use of oxygen/argon ratios to estimate bioflux.

5.3.1 Cumulative fluxes

Compared to the changes in NCP at different distances offshore (i.e. high NCP over the shelf), cumulative bioflux is relatively similar at all distances offshore (Figure 5.7b,d,f). Total cumulative bioflux out of the ocean at these three distances offshore only ranges from 730 to 1170 mmol m^{-2} while NCP ranges over an order of magnitude from 743 to 7590 mmol m^{-2}. This discrepancy is caused by the upwelling of water undersaturated in oxygen which reduces oxygen outgassing or even causes an influx of oxygen from the atmosphere into the mixed layer. This effect can be seen most clearly at around mid-September, coinciding with the large upwelling favourable wind event, where there is a decrease in the cumulative bioflux as oxygen is actually added to the mixed layer from the atmosphere.

As mentioned above (section 3.2.4), most of my calculated entrainment term is included in the vertical diffusion fluxes, and the two lines generally follow each other, with the difference between entrainment and vertical diffusion being the excess bio-

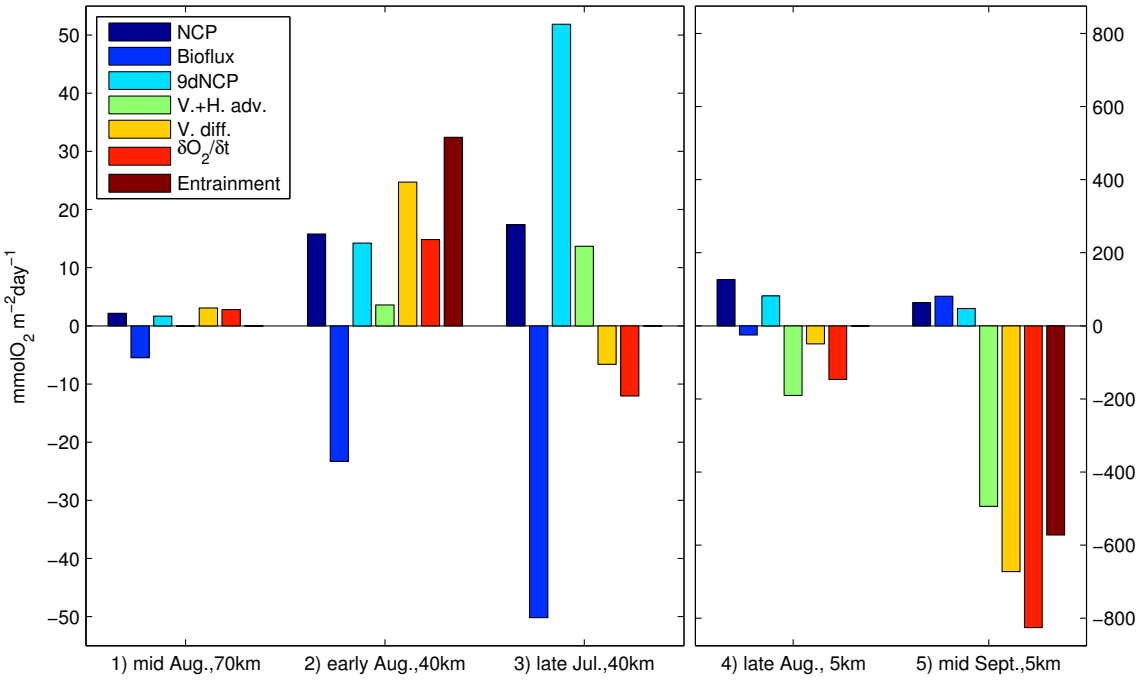

Figure 5.6: Bars represent biological fluxes in the mixed layer as described by the legend (section 3.2.4) for different points in time and different distances offshore (Figure 5.2). Examples of 1) an open ocean-like situation, 2) a situation in which change in the mixed layer depth causes bioflux to overestimate NCP, 3) a situation in which temporal and spatial averaging of NCP is effective, 4) a situation in which the oxygen saturation is positive but still being affected by the upwelling signal, and 5) a situation in which bioflux is affected by low oxygen water due to upwelling. Scale changes between the left and right side of the plot. Note that bioflux is a described as a flux out of the mixed layer and is shown here as a negative flux.

logical oxygen remaining in the model box or boxes added to the mixed layer after mixing has occurred. Over the course of the run, entrainment is generally a source of oxygen to the mixed layer offshore due to net productivity and biological oxygen supersaturation below the mixed layer, which is entrained when the mixed layer deepens. The most obvious example of this entrainment occurs just past the middle of August (Figure 5.7a,c), where the mixed layer has stayed relatively shallow for the previous few weeks, and NCP has been occurring below the mixed layer. When the mixed layer deepens, biological oxygen is entrained into the mixed layer raising the amount of biological oxygen in the mixed layer. By contrast, most of the NCP within 5 km from shore occurs within the mixed layer, and undersaturated waters are entrained when the mixed layer deepens (Figure 5.7e,f). When the mixed layer becomes

shallower again, biological oxygen is trapped below the mixed layer, and consumed by respiration rather than released to the atmosphere through gas exchange.

5.4 Using bioflux as a proxy for NCP

The area where bioflux and 9dNCP, calculated as described above, have the highest correlation is far offshore where there is less productivity, and where productivity farther onshore and gas exchange have begun to erase the upwelling signal (Figure 5.8). Upwelling favourable winds advect water offshore; however, by the time this water has left the shelf, most of the excess nutrients due to upwelling have been consumed by primary productivity. As a result there is less productivity offshore of the shelf break in general, but more importantly, oxygen concentration is closer to equilibrium. Therefore, any local production is more likely to be accurately detected by bioflux; e.g. my example (1) in mid-August, 70 km offshore (Figure 5.6). Over the shelf, where these nutrients are being consumed, bioflux is low or negative due to the upwelling of water undersaturated in oxygen. Despite the fact that productivity is occurring, the undersaturated water causes an influx of oxygen from the atmosphere in an attempt to restore equilibrium which translates as negative bioflux, and even over the shelf, the best correlations are found nearer to the shelf break and the worst closest to the shore where upwelling is strongest (Figure 5.8a).

Inaccuracies in positive bioflux When the estimated bioflux is negative it is simple to throw out the data as having been affected by the upwelling signal, such as the example point (5) in mid September, 5 km offshore (Figure 5.6). However, when the signal is positive, that does not ensure that the upwelling signal has been entirely erased; e.g. my example (4) in late August around 5 km offshore (Figure 5.6). Since bioflux only accounts for the excess biologically produced oxygen above equilibrium, much of the NCP remains unaccounted for in this type of situation. These scenarios fall in the upper left corner of NCP vs Bioflux plots (Figure 5.8), where NCP is high and bioflux is low. Comparing temporally and spatially averaged NCP (9dNCP) to bioflux improves the correlation of the points where bioflux is greater than NCP, because the averaging helps account for the lag effect, but averaging cannot account for the injection of low oxygen water into the mixed layer.

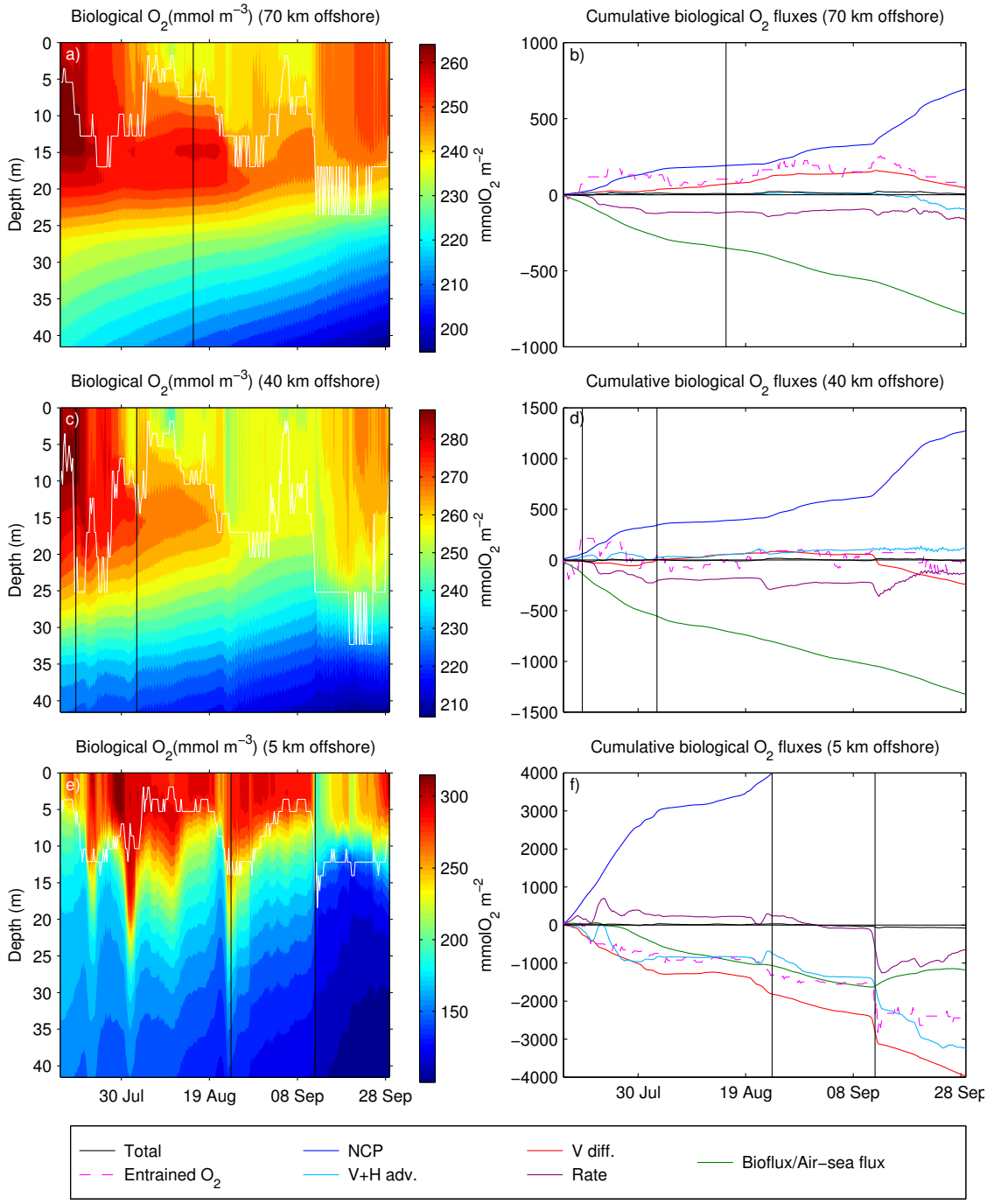

Figure 5.7: Base run: Biological oxygen concentration ($(\Delta O_2/Ar + 1) \cdot [O_2]_{eq}$) and mixed layer depth (white line) as a function of time for a) 70 km offshore (example 1), c) 40 km offshore (examples 3, 2), and e) 5 km offshore (examples 4, 5). Black lines represent the time points of interest. Cumulative O_2 fluxes for b) 70 km offshore, d) 40 km offshore, and f) 5 km offshore. Colour bars (left panels) and y-axes (right panels) are different scales at different distances offshore.

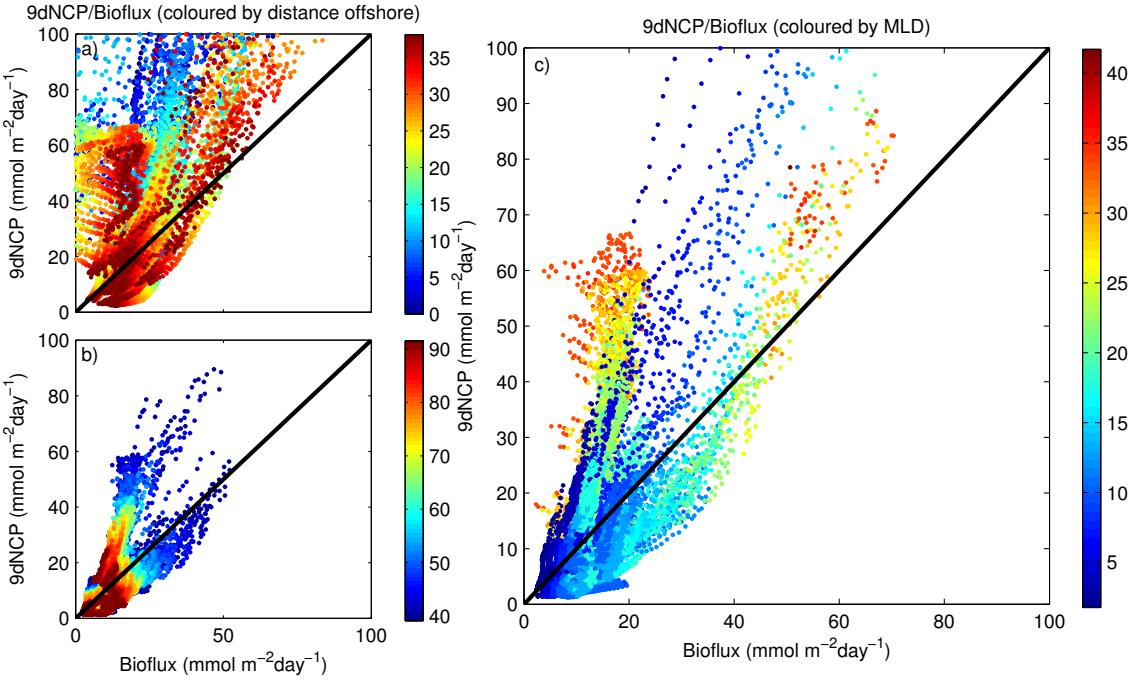

Figure 5.8: Bioflux plotted vs 9dNCP a) onshore (1-40 km) and b) offshore (40-90 km) colour coded by distance offshore. c) Bioflux plotted vs 9dNCP 25-90 km colour coded by MLD. The black line represents the 1:1 relationship between bioflux and 9dNCP in all plots.

5.4.1 Advection of upwelled water

The furthest absolute distance a water parcel is advected offshore over 9 days is about 25 km (maximum cross-shore velocity $\sim$3 cm s^{-1} associated with the mid-September upwelling event)(Figure 5.3 b). Since the NCP averaging period of 9 days is based on the residence time with respect to gas exchange, I can say that past 25 km offshore of the upwelling plume, the low oxygen upwelling signal is largely erased given typical wind forcing in this region. I conclude that comparisons of bioflux to NCP will be most accurate past 25 km offshore (Figure 5.8c). There are points within 25 km of shore in which bioflux accurately estimates NCP, but 80 percent of the discarded values have differences of greater than 10 mmol m^{-2}day^{-1} (33% of the 9dNCP value). The upwelling in this model occurs right at the shore. However, upwelling does not always occur directly at the coast, and in those situations, the distance over which bioflux is most inacurate should be calculated from the offshore edge of the upwelling plume. Most of the data from the shore to 25 km offshore have high NCP (60-100 mmol m^{-2}day^{-1}) and low bioflux (0-20 mmol m^{-2}day^{-1}) which corresponds to values

in which bioflux is positive, but the concentration of oxygen in the mixed layer is still being affected by the addition of low oxygen water due to upwelling such as my example (4) in late August, 5 km offshore (Figure 5.6). These points are found in the upper left corner in Figure 5.8a and are no longer present once data from the first 25 km onshore are removed (Figure 5.8c). Ignoring data from the first 25 km onshore, bioflux tends to both overestimate and underestimate NCP so that overall values agree. The mean of all bioflux leaving the mixed layer and the associated NCP values are 18.72 and 30.47 mmol $m^{-2}day^{-1}$, respectively (a percent difference of 39%). With the 25 km of onshore values removed, mean bioflux and NCP values are 13.02 and 14.75 mmol $m^{-2}day^{-1}$, respectively (a percent difference of 12%).

Note that changing the shelf width in my model did not significantly influence this result. The maximum advection distance is 22.7 km with a narrower shelf (30 km), 24.9 km with a wider shelf (70 km), and 23.0 km with a shallow shelf (min depth 39 m, shelf width 40 km) with a similar distribution of advection distances as seen in the base run (Appendix C). In contrast, higher wind forcing increased these advective distances in the model, as seen in runs from 2004 and 2008, both years with higher wind forcing than the base run (Appendix D). Runs performed using forcing from 2004 and 2008 have maximum advection distances of 37.5 and 34.9 km, respectively (with mean residence times with respect to gas exchange of 7 days). Therefore the strength of wind forcing, not shelf bathymetry, influences the location relative to the upwelling plume at which bioflux can be used as a proxy for temporally and spatially averaged NCP (Appendix C, D).

My model domain is not large enough to model some wider upwelling shelves, such as the Canary current upwelling system where the inner shelf (defined as onshore of the 100 m isobath) can be up to 250 km wide (Carr and Kearns, 2003). Based on the range of shelf widths in the 4 major upwelling regions of the world, the model bathymetry falls in the narrower range of shelf widths; therefore my conclusions would be more uncertain for medium to wide shelves. However, parts of the major shelves, especially the California shelf, remain narrower (10 - 20 km wide) (Carr and Kearns, 2003), and my model could be generalized to those regions. Wind forcing is variable among major upwelling regions. In the Canary Islands upwelling zone, where the shelf can get up to 250 km wide, there are wind speeds up to 20 m s^{-1} (Barton et al., 1998), whereas the summer winds along the Oregon and California coast tend fall between 5 and 10 m s^{-1} (Tinis et al., 2006) which is closer to the range of wind forcing used in in my model (mean = 5 m s^{-1}).

5.4.2 Low NCP and deep mixed layers

With the first 25 km onshore removed to ensure that the effects of the upwelling plume are removed, I investigated what other data should be eliminated to provide a higher correlation of bioflux to temporally and spatially averaged NCP. At lower values of bioflux (bioflux < 20 mmol $m^{-2}day^{-1}$), the percentage error (difference between bioflux and 9dNCP divided by 9dNCP) is fairly high because the values involved are small. However if a given bioflux value is less than 20 mmol $m^{-2}day^{-1}$, 83% of the corresponding 9dNCP values are also found between 0 and 20 mmol $m^{-2}day^{-1}$ in the base run, 81% in the run with 2004 forcing, but only 16% in the run with 2008 forcing. 2008 had a higher frequency of stronger upwelling favourable wind events, which generally causes overall underestimation of NCP by bioflux. However, if there has not been a recent upwelling event (within approximately 9 days) or recent change in mixed layer depth, observations of bioflux values of less than 20 mmol $m^{-2}day^{-1}$ can generally be assumed to indicate temporally and spatially averaged NCP values in the same range.

In addition, bioflux is most accurate as a predictor of NCP when mixed layer depths are less than 25 m deep (Figure 5.8). Deeper mixed layers take longer to ventilate and could create a larger lag effect causing underestimation of NCP by bioflux, especially if the deep mixed layer is associated with a low gas transfer velocity. This situation is seen in mid to late September, which is the location most of the points removed using this criteria are associated with. While removing values with a mixed layer depth greater than 25 m does remove points in which bioflux significantly underestimates NCP, it also removes some points in which bioflux is a good proxy for NCP. In the base run, 61% of the points removed based on mixed layer depths greater than 25 m deep were points with a percent difference between bioflux and NCP greater than $\pm 50\%$.

5.4.3 Testing for other exclusion criteria

In addition to colour coding the correlation of bioflux with 9dNCP by mixed layer depth and by distance offshore (Figure 5.8), I also investigated the use of temperature, time, chlorophyll, residence time with respect to gas exchange, change in mixed layer depth, wind speed, and pCO_2 to sort the data (not shown). None of these indicators clearly highlight points that should be excluded. Higher temperatures tend to have lower 9dNCP and bioflux associated with them, but that is due to higher temperatures

in the model runs performed being found offshore which causes similar patterns to be seen as when the data is sorted by distance. Both time and residence time with respect to gas exchange highlight the many offshoot points in which bioflux underestimates NCP significantly, but those points are all associated with the last portion of the run following the mid-September major upwelling event where mixed layers are deep and gas transfer velocities low. Chlorophyll and change in mixed layer depth showed no discernible pattern. Sorting by wind speed looked similar to sorting by mixed layer depth at higher values, and otherwise showed little discernible pattern. Lastly, pCO_2 did show a correlation between the highest pCO_2 values and negative bioflux; however, since negative bioflux points are already eliminated by the community, this result did not improve my exclusion criteria.

5.5 Limitations and assumptions

There are limitations involved in the use of models to explore questions about the ocean. For example, the model is quasi 2D representing a 90 km (cross-shelf) by 5 km (along-shelf) transect with uniform values alongshore which assumes a zero alongshore gradient. Near the VI transects, alongshore advection speeds are typically in the range of 20 cm s^{-1}, which over the course of the residence time with respect to gas exchange (9 days), corresponds to an alongshore distance travelled of 150 km. Therefore I must assume that alongshore values are nearly uniform over 150 km. While this assumption of uniformity may not be valid at times, significant regions of the west coast Vancouver Island often have similar levels of chlorophyll over these distance scales (Gower, 2004). Another consequence of a quasi 2D model is that it cannot model mesoscale variability, which can be important in driving production in coastal regions (Mahadevan and Tandon, 2006). Some important upwelling shelves in the world (e.g the Canary Islands) are wider than the entire domain of my model and further studies need to be done using a model able to simulate wider shelves and assess O_2/Ar dynamics in these regions. In general, models have a tendency to drift over time, and this model is no exception. For example, there is no freshwater input from either precipitation or river water, causing salinity to increase over the course of the run. During the summer in the forcing location, the lack of precipitation is a reasonable assumption because precipitation is generally low during the time over which the model is running. The study region also contains the VICC which adds fresh water to the system via mixing. The VICC is not modelled. The time period

over which results can be analyzed is controlled by a balance between the time needed for spinup and weighting of the gas transfer velocity, and the point where summer upwelling ceases and model drift becomes significant. A 3D model covering a larger domain and with the ability to run over a longer time period would account for most of these limitations (apart from model drift), but the complexity added is significant and beyond the scope of this study. Adding precipitation or restoring of values to prevent significant drift would be a good first step.

Chapter 6

Conclusions

Based on this study, bioflux can be used in coastal upwelling zones as a lower bound for NCP spatially and temporally averaged over the residence time of oxygen in the mixed layer under certain conditions. The current practice of ignoring values with negative bioflux (biological flux of oxygen into the ocean) is reasonable, but I suggest several other situations in which bioflux data should be excluded. In the base run, averaging temporally and spatially over the residence time due to gas exchange (9 days) accounts for horizontal advection, but bioflux is still only a good estimate of NCP if physical fluxes of oxygen into and out of the box are approximately equal. If the amount of oxygen entering and exiting the mixed layer boxes is not equal, then there will be a discrepancy between bioflux and temporally and spatially averaged NCP. This effect is commonly seen when the mixed layer deepens, entraining either high or low oxygen waters from below the mixed layer. Therefore, data in such situations is unreliable in terms of estimating NCP in the mixed layer, although, when water with high biological oxygen is entrained, bioflux can indicate net productivity occurring below the mixed layer. Bioflux observations within the nearshore zone are likely to significantly underestimate NCP. Past the maximum distance water is advected from the offshore edge of the upwelling plume (base run = 25 km), the effects of upwelling have decreased. In addition, I found that offshore of 25 km when bioflux is less than 20 mmol m^{-2} day^{-1}, NCP is also often within the same range. For offshore bioflux values higher than 20 mmol m^{-2} day^{-1}, the best correlation is seen when mixed layer depths are shallower than 25 m. For these bioflux values above 20 mmol m^{-2} day^{-1}, there is a 24% difference between the mean bioflux and 9dNCP (bioflux and 9dNCP averaged over all points temporally and spatially, and the percent difference between the two averages); however, eliminating deeper mixed layer depth data decreased the

difference to just 8% in the base run(Table 6.1).

Model runs were also performed using forcing conditions from other years and with different shelf widths to determine the sensitivity of these results to the base run (Appendix C, D). The magnitude of the improvement due to cutting off values associated with deeper MLDs is different depending on the run - 2004 shows little change in the difference between mean NCP and bioflux values since there are few MLDs greater than 25 m to remove, but 2008 shows improvement. (Table 6.1). The removal of MLDs does not make the correlation any worse for either run. The 2004 run changes very slightly (bioflux still overestimates NCP by 29%), and bioflux in the 2008 run underestimates bioflux by 27% with MLDs greater than 25 m removed, rather than 32% with those points counted. Decreasing the cutoff depth to 20 m for all runs makes the results from the 2008 run better (23%) but the 1993 and 2004 runs slightly worse (9% and 30%, respectively). Since I only have these runs for forcing from three different years, I cannot make a specific statement on the effect of MLD on the underestimation of spatially and temporally averaged NCP by bioflux, but it is possible that the maximum mixed layer depth at which data should be cut off is a function of the mean wind forcing.

Bioflux continually underestimates temporally and spatially averaged NCP in all runs performed and can still be used as a lower bound, but data collected during strong upwelling periods are more likely to underestimate temporally and spatially averaged NCP. Changes in shelf width have little effect on the distance offshore at which the upwelling effect is reduced - a 70 km wide shelf showed no change in distance, while a 30 km wide shelf showed only a difference of 3 km.

In short, the oxygen/argon method cannot be effective in coastal upwelling zones without the collection of other data relating to the state of the ocean both previous to and at the time of collection (wind speed over the past 30 days, mixed layer depth, and distance from the upwelling plume). Further study could be done regarding the inclusion of points that are nearer to shore than the maximum advection distance but that are more than 9 days removed from an upwelling favourable wind event. Such exclusion criteria could be applied observationally using the upwelling index. This study was conducted using a quasi 2D model and as such is unable to cover the effects of 3D dynamics such as eddies, which remains another area for further investigation. The expansion of this study to other shelf types which are more similar to the wider upwelling coasts, such as the Canary Islands, as well as the use of wind forcing from other locations would improve the understanding of the sensitivity of this method to

these factors. Furthermore, examining the elimination of a percentage of the deepest mixed layer depths rather than mixed layer depths greater than a fixed depth may lead to better application of this method across various locations and times. Finally, the frequency over which measurements should be taken in order to better understand the link between NCP and carbon export should be explored.

Table 6.1: Wind forcing in units of N m^{-2}. Events are defined as a point in time or a group of consecutive points in time where wind forcing $> \pm$ 0.2. The peak is the maximum wind forcing (positive or negative). Comparison between mean bioflux and mean temporally and spatially averaged NCP (in units of mmol m^{-2} day^{-1}) over the full model domain and over the course of the run. Runs shown include runs with different bathymetry and wind forcing. Each data exclusion criterium also excludes points based on all data exclusion criteria listed above it in the table. When a value of bioflux is excluded, the NCP value associated with that location and time is also excluded.

Year:	1993	1993	1993	1993	2004	2008
Bathymetry:	base	wide shelf	narrow shelf	shallow shelf	base	base
Wind forcing						
mean	-0.0179	-0.0179	-0.0179	-0.0179	-0.0190	-0.0238
max peak	-0.3536	-0.3536	-0.3536	-0.3536	-0.2462	-0.4866
no. events	3	3	3	3	3	7
Negative bioflux excluded						
bioflux	18.72	18.51	19.43	18.81	20.30	26.32
NCP	30.47	29.51	30.50	33.48	29.91	43.59
Values where distance offshore $<$ max. advection distance excluded						
bioflux	13.02	12.23	15.26	13.43	12.85	21.31
NCP	14.75	12.68	18.14	15.76	12.99	29.55
Bioflux $<$ 20 mmol m^{-2} day^{-1} excluded						
bioflux	30.71	32.15	31.51	24.77	26.75	31.70
NCP	38.00	38.24	41.85	26.90	20.78	43.68
Values where MLD $>$ 25 m excluded						
bioflux	29.35	29.47	29.44	24.64	26.64	33.69
NCP	31.63	32.21	36.71	25.60	20.69	49.82

Bibliography

Barth, J. A. and Wheeler, P. A. (2005). Introduction to special section: coastal advances in shelf transport. *Journal of Geophysical Research: Oceans (1978–2012)*, 110(C10).

Barton, E., Arıstegui, J., Tett, P., Cantón, M., Garcıa-Braun, J., Hernández-León, S., Nykjaer, L., Almeida, C., Almunia, J., Ballesteros, S., et al. (1998). The transition zone of the Canary Current upwelling region. *Progress in Oceanography*, 41(4):455–504.

Bianucci, L. (2010). *Carbon, oxygen, and nitrogen cycles on the Vancouver Island shelf*. PhD thesis, University of Victoria.

Bianucci, L., Denman, K. L., and Ianson, D. (2011). Low oxygen and high inorganic carbon on the Vancouver Island shelf. *Journal of Geophysical Research: Oceans (1978–2012)*, 116(C7).

Botsford, L. W., Lawrence, C. A., Dever, E. P., Hastings, A., and Largier, J. (2006). Effects of variable winds on biological productivity on continental shelves in coastal upwelling systems. *Deep-Sea Research*, 2(53):3116–3140.

Cai, W.-J., Dai, M., and Wang, Y. (2006). Air-sea exchange of carbon dioxide in ocean margins: A province-based synthesis. *Geophysical Research Letters*, 33(12).

Carr, M.-E. and Kearns, E. J. (2003). Production regimes in four eastern boundary current systems. *Deep Sea Research Part II: Topical Studies in Oceanography*, 50(22):3199–3221.

Cassar, N., Barnett, B. A., Bender, M. L., Kaiser, J., Hamme, R. C., and Tilbrook, B. (2009). Continuous high-frequency dissolved O_2/Ar measurements by equilibrator inlet mass spectrometry. *Analytical Chemistry*, 81(5):1855–1864.

Crawford, W. R. and Dewey, R. K. (1989). Turbulence and mixing: Sources of nutrients on the Vancouver Island continental shelf. *Atmosphere-Ocean*, 27:428–442.

Crawford, W. R. and Peña, M. A. (2013). Declining oxygen on the british columbia continental shelf. *Atmosphere-Ocean*, 51(1):88–103.

Emerson, S. (2014). Annual net community production and the biological carbon flux in the ocean. *Global Biogeochemical Cycles*, 28(1):14–28.

Emerson, S., Quay, P., Stump, C., Wilbur, D., and Schudlich, R. (1995). Chemical tracers of productivity and respiration in the subtropical Pacific Ocean. *Journal of Geophysical Research: Oceans (1978–2012)*, 100(C8):15873–15887.

Emerson, S., Stump, C., Wilbur, D., and Quay, P. (1999). Accurate measurement of O_2, N_2, and Ar gases in water and the solubility of N_2. *Marine Chemistry*, 64(4):337–347.

Fennel, K., Brady, D., DiToro, D., Fulweiler, R. W., Gardner, W. S., Giblin, A., McCarthy, M. J., Rao, A., Seitzinger, S., Thouvenot-Korppoo, M., et al. (2009). Modeling denitrification in aquatic sediments. *Biogeochemistry*, 93(1-2):159–178.

Fennel, K., Wilkin, J., Levin, J., Moisan, J., O'Reilly, J., and Haidvogel, D. (2006). Nitrogen cycling in the Middle Atlantic Bight: Results from a three-dimensional model and implications for the North Atlantic nitrogen budget. *Global Biogeochemical Cycles*, 20(3).

Fennel, K., Wilkin, J., Previdi, M., and Najjar, R. (2008). Denitrification effects on air-sea CO_2 flux in the coastal ocean: Simulations for the northwest North Atlantic. *Geophysical Research Letters*, 35(24).

Freeland, H. J., Crawford, W. R., and Thomson, R. E. (1984). Currents along the Pacific coast of Canada. *Atmos.-Ocean.*, 22:151–172.

Garcia, H. E. and Gordon, L. I. (1992). Oxygen solubility in seawater: Better fitting equations. *Limnology and Oceanography*, 37(6):1307–1312.

Garcia, H. E. and Gordon, L. I. (1993). Erratum: Oxygen solubility in seawater: Better fitting equations. *Limnology and Oceanography*, 38(3):656.

Giesbrecht, K. E., Hamme, R. C., and Emerson, S. R. (2012). Biological productivity along Line P in the subarctic northeast Pacific: In situ versus incubation-based methods. *Global Biogeochemical Cycles*, 26.

Gower, J. F. (2004). SeaWiFS global composite images show significant features of canadian waters for 1997–2001ers for 1997-2001. *Canadian Journal of Remote Sensing*, 30(1):26–35.

Hales, B., Karp-Boss, L., Perlin, A., and Wheeler, P. A. (2006). Oxygen production and carbon sequestration in an upwelling coastal margin. *Global Biogeochemical Cycles*, 20.

Hamme, R. C., Cassar, N., Lance, V. P., Vaillancourt, R. D., Bender, M. L., Strutton, P. G., Moore, T. S., DeGrandpre, M. D., Sabine, C. L., Ho, D. T., et al. (2012). Dissolved O_2/Ar and other methods reveal rapid changes in productivity during a Lagrangian experiment in the Southern Ocean. *Journal of Geophysical Research: Oceans (1978–2012)*, 117(C4).

Hamme, R. C. and Emerson, S. R. (2004). The solubility of neon, nitrogen and argon in distilled water and seawater. *Deep Sea Research Part I: Oceanographic Research Papers*, 51(11):1517–1528.

Hamme, R. C. and Severinghaus, J. P. (2007). Trace gas disequilibria during deep-water formation. *Deep Sea Research Part I: Oceanographic Research Papers*, 54(6):939–950.

Harrison, W. G., Platt, T., and Lewis, M. R. (1987). f-ratio and its relationship to ambient nitrate concentration in coastal waters. *Journal of Plankton Research*, 9(1):235–248.

Hendricks, M. B., Bender, M. L., and Barnett, B. A. (2004). Net and gross O_2 production in the Southern Ocean from measurements of biological O_2 saturation and its triple isotope composition. *Deep Sea Research Part I: Oceanographic Research Papers*, 51(11):1541–1561.

Hickey, B., Thomson, R. E., Yih, H., and LeBlond, P. H. (1991). Velocity and temperature fluctuations in a buoyancy-driven current off Vancouver Island. *Journal of Geophysical Research: Oceans*, 96:10507–10538.

Hickey, B. M. and Banas, N. S. (2008). Why is the northern end of the California current system so productive? *Oceanography*, 21(4):90–107.

Ho, D. T., Law, C. S., Smith, M. J., Schlosser, P., Harvey, M., and Hill, P. (2006). Measurements of air-sea gas exchange at high wind speeds in the southern ocean: Implications for global parameterizations. *Geophysical Research Letters*, 33(16).

Ianson, D. and Allen, S. E. (2002). A two-dimensional nitrogen and carbon flux model in a coastal upwelling region. *Global Biogeochemical Cycles*, 16(1):11–1.

Ianson, D., Feely, R. A., Sabine, C. L., and Juranek, L. W. (2009). Features of coastal upwelling regions that determine net air-sea CO_2 flux. *Journal of Oceanography*, 65(5):677–687.

Jonsson, B., Salisbury, J., and Mahadevan, A. (2011). Large variability in continental shelf production of phytoplankton carbon revealed by satellite. *Biogeosciences*, 8:1213–1223.

Jonsson, B. F., Doney, S. C., Dunne, J., and Bender, M. (2013). Evaluation of the southern ocean O_2/Ar-based NCP estimates in a model framework. *Journal of Geophysical Research: Biogeosciences*, 118(2):385–399.

Kaiser, J., Reuer, M. K., Barnett, B., and Bender, M. L. (2005). Marine productivity estimates from continuous O_2/Ar ratio measurements by membrane inlet mass spectrometry. *Geophysical Research Letters*, 32(19).

Kundu, P. K. and Thomson, R. E. (1990). Inertial oscillations observed near British Columbia. *Pure and Applied Geophysics*, 133(4):677–689.

Laws, E. A. (1991). Photosynthetic quotients, new production and net community production in the open ocean. *Deep Sea Research Part A. Oceanographic Research Papers*, 38(1):143–167.

Mackas, D. L. (1992). Seasonal cycle of zooplankton off southwestern British Columbia: 1979-89. *Canadian Journal of Fisheries and Aquatic Sciences*, 49(5):903–921.

Mahadevan, A. and Tandon, A. (2006). An analysis of mechanisms for submesoscale vertical motion at ocean fronts. *Ocean Modelling*, 14(3):241–256.

Nemcek, N., Ianson, D., and Tortell, P. D. (2008). A high-resolution survey of DMS, CO_2, and O_2/Ar distributions in productive coastal waters. *Global Biogeochemical Cycles*, 22(2).

Nicholson, D. P., Stanley, R. H., Barkan, E., Karl, D. M., Luz, B., Quay, P. D., and Doney, S. C. (2012). Evaluating triple oxygen isotope estimates of gross primary production at the Hawaii Ocean Time-series and Bermuda Atlantic Time-series study sites. *Journal of Geophysical Research: Oceans (1978–2012)*, 117(C5).

Peterson, B. J. (1980). Aquatic primary productivity and the ^{14}C-CO_2 method: A history of the productivity problem. *Annual Review of Ecology and Systematics*, pages 359–385.

Quay, P., Peacock, C., Björkman, K., and Karl, D. (2010). Measuring primary production rates in the ocean: Enigmatic results between incubation and non-incubation methods at station ALOHA. *Global Biogeochemical Cycles*, 24(3).

Raymond, W. H. and Kuo, H. (1984). A radiation boundary condition for multi-dimensional flows. *Quarterly Journal of the Royal Meteorological Society*, 110(464):535–551.

Reuer, M. K., Barnett, B. A., Bender, M. L., Falkowski, P. G., and Hendricks, M. B. (2007). New estimates of Southern Ocean biological production rates from O_2/Ar ratios and the triple isotope composition of O_2. *Deep-Sea Research*, 54:951–974.

Ryther, J. H. (1986). Photosynthesis and fish production in the sea. *Readings in Marine Ecology*, page 97.

Shchepetkin, A. F. and McWilliams, J. C. (2005). The regional oceanic modeling system (ROMS): a split-explicit, free-surface, topography-following-coordinate oceanic model. *Ocean Modelling*, 9(4):347–404.

Siegenthaler, U. and Sarmiento, J. L. (1993). Atmospheric carbon dioxide and the ocean. *Nature*, 395:119–125.

Smith, R. L. (1994). The physical processes of coastal ocean upwelling systems. In Summerhayes, C. P., Emeis, K.-C., Angel, M. V., Smith, R. L., and Zeitzschel, B., editors, *Upwelling in the ocean: Modern processes and ancient records*, pages 39–64. Wiley and Sons Ltd.

Smith, S. D. (1988). Coefficients for sea surface wind stress, heat flux, and wind profiles as a function of wind speed and temperature. *Journal of Geophysical Research: Oceans (1978–2012)*, 93(C12):15467–15472.

Spitzer, W. S. and Jenkins, W. J. (1989). Rates of vertical mixing, gas exchange and new production: Estimates from seasonal gas cycles in the upper ocean near Bermuda. *Journal of Marine Research*, 47(1):169–196.

Stanley, R. H., Kirkpatrick, J. B., Cassar, N., Barnett, B. A., and Bender, M. L. (2010). Net community production and gross primary production rates in the western equatorial Pacific. *Global Biogeochemical Cycles*, 24(4).

Steemann Nielsen, E. (1952). The use of radioactive carbon (C^4) for measuring organic production in the sea. *J. Cons., Cons. Perm. Int. Explor. Mer*, 18:117–140.

Thomson, R. E. and Fine, I. V. (2003). Estimating mixed-layer depth from oceanic profile data. *Journal of Atmospheric and Oceanic Technology*, 20:319–329.

Thomson, R. E., Hickey, B. M., and LeBlond, P. H. (1989). The Vancouver Island coastal current: fisheries barrier and conduit. In McFarlane, G. A., editor, *Effects of ocean variability on recruitment and an evaluation of parameters used in stock assessment models*, volume 108, pages 265–296. Can. Spec. Publ. Fish. Aquat. Sci.

Tinis, S. W., Thomson, R. E., Mass, C. F., and Hickey, B. M. (2006). Comparison of MM5 and meteorological buoy winds from British Columbia to northern California. *Atmosphere-Ocean*, 44(1):65–81.

Tortell, P. D., Merzouk, A., Ianson, D., Pawlowicz, R., and Yelland, D. R. (2012). Influence of regional climate forcing on surface water pCO_2, Δ O_2/Ar and dimethylsulfide (DMS) along the southern british columbia coast. *Continental Shelf Research*, 47:119–132.

Uitz, J., Claustre, H., Morel, A., and Hooker, S. B. (2006). Vertical distribution of phytoplankton communities in open ocean: An assessment based on surface chlorophyll. *Journal of Geophysical Research*, 111.

Volk, T. and Hoffert, M. I. (1985). Ocean carbon pumps: analysis of relative strengths and efficiencies in ocean-driven atmospheric pCO_2 changes. In Sundquist, E. T. and Broecker, W. S., editors, *The carbon cycle and atmospheric CO_2, natural variations*

archean to present, volume AGU Monograph 32, pages 99–110, Washington, D.C. AGU.

Walsh, J. J., Dieterle, D. A., and Pribble, J. R. (1991). Organic debris on the continental margins: a simulation analysis of source and fate. *Deep Sea Research Part A. Oceanographic Research Papers*, 38(7):805–828.

Wanninkhof, R. (1992). Relationship between wind speed and gas exchange over the ocean. *Journal of Geophysical Research: Oceans (1978–2012)*, 97(C5):7373–7382.

Ware, D. M. and Thomson, R. E. (2005). Bottom-up ecosystem trophic dynamics determine fish production in the Northeast Pacific. *Science*, 308(5726):1280–1284.

Weiss, R. (1974). Carbon dioxide in water and seawater: the solubility of a non-ideal gas. *Marine Chemistry*, 2(3):203–215.

Appendix A

Dissolved gas sensitivity

This project was concerned primarily with the air-sea gas exchange of biological oxygen at the ocean surface. To test how much of an effect the initial conditions had on my final result, I performed two sensitivity runs. In the first, oxygen and argon concentrations were initialized to 0 mmol m^{-3} in the upper 8 boxes. Oxygen and argon concentrations approached base run values in an exponential fashion, and by day 20, the mean over the model spatial domain for oxygen and argon had reached 82% and 81% of the mean in the base run, respectively (Figure A.1, A.2)). Oxygen in the base run is initialized as the summer mean of all available vertically variable profiles on the VI transect, and argon is initialized at equilibrium, which are values much closer to real ocean concentrations than the initialization values in this sensitivity run.

To simplify the effects on the ratio $\Delta O_2/Ar$, I performed another sensitivity run in which only oxygen was set to zero in the surface box, while argon concentrations remained the same as those in the shallow shelf run. This sensitivity run is performed with the shallow shelf bathymetry, and bioflux is compared with the bioflux from the shallow shelf bathymetry run (Appendix C). Bioflux values cannot be interpreted until all values involved in the calculation are past the spinup time. Oxygen and argon have spinup times of 20 days, and in addition to that, the gas transfer velocity accounts for past variability in gas fluxes which affect the current $\Delta O_2/Ar$. Therefore, the spinup time for oxygen and argon should not overlap with the 30 day weighting time for k_{O_2}, and analysis of bioflux should begin on day 50. By this time, the mean over the model spatial domain for bioflux had reached 78% of the mean in the shallow shelf run (Figure A.3, A.4)).

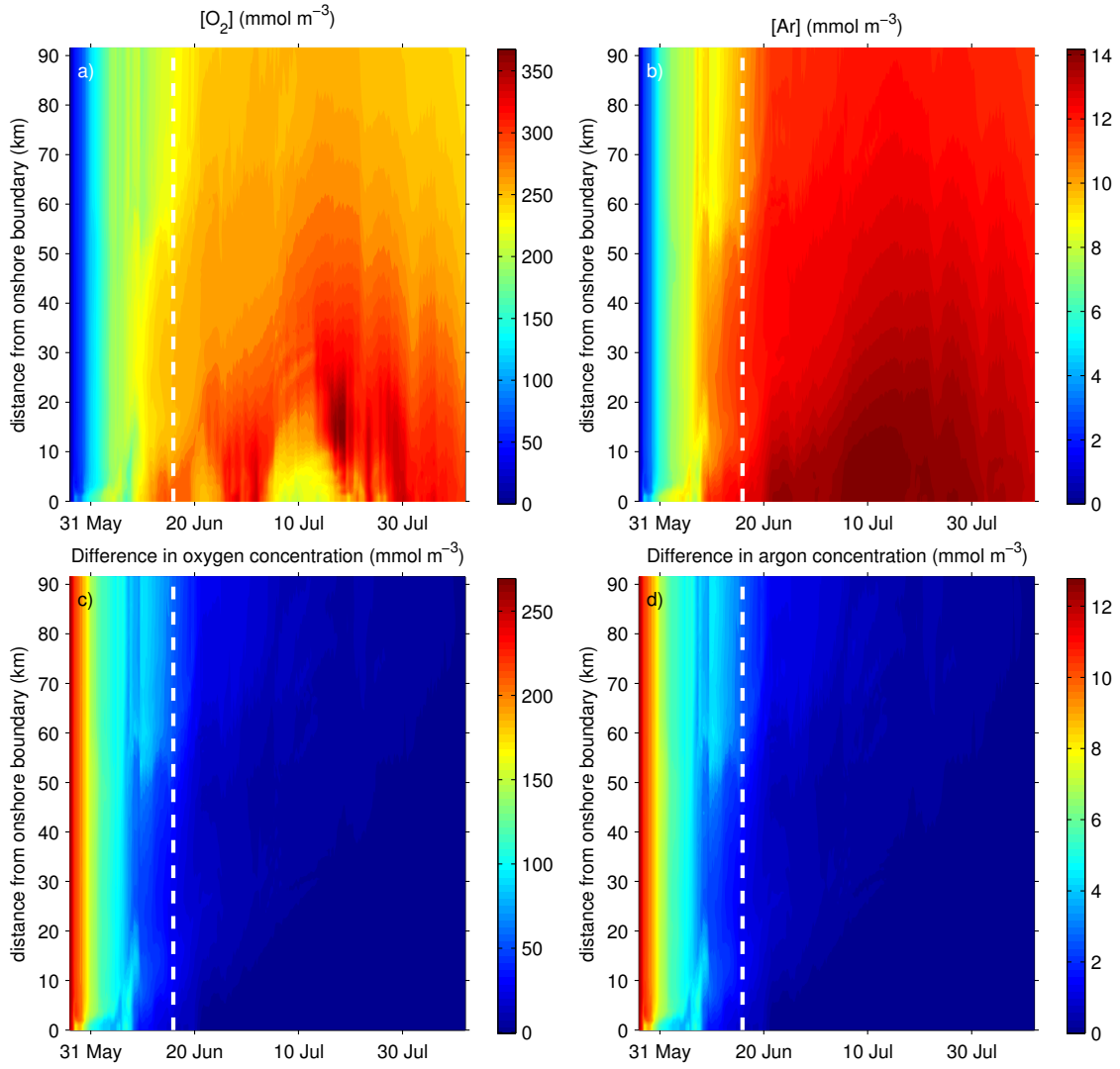

Figure A.1: Property plots within 90 km of the shore over the course of the first sensitivity run (1993) where both oxygen and argon were set to zero in the upper 8 boxes. a) Oxygen concentration in the sensitivity run, b) Argon concentration in the sensitivity run, c) difference between oxgyen concentrations in the base and sensitivity runs, and d) difference between argon concentrations in the base and sensitivity runs. Note the x-axis - this plot shows the spinup time (day 1 - 20), weighting time (day 20 - 50), and the 25 days after the spinup and weighting time. White dotted line indicates the end of the spinup time.

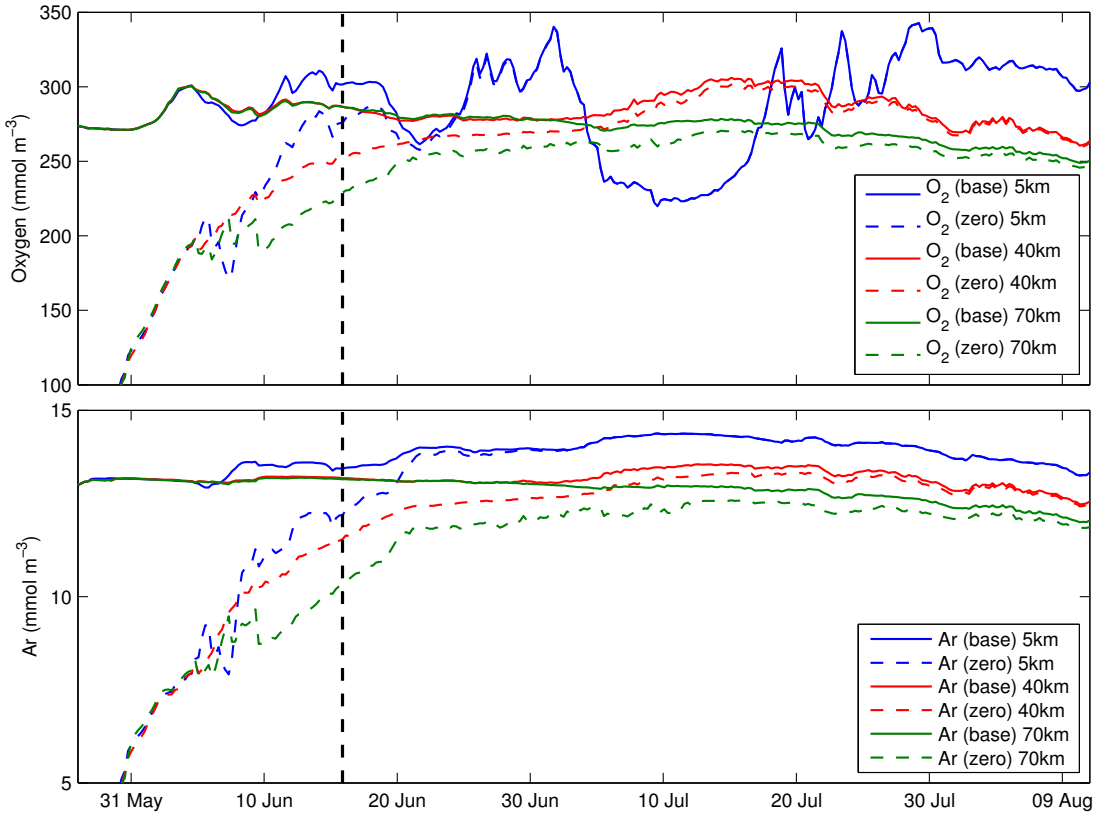

Figure A.2: a) Oxygen concentration, and b) Argon concentration in the mixed layer over the course of the run in Figure A.1 and in the base run at 5km offshore, 40 km offshore, and 70 km offshore. Black line represents the end of the spinup time.

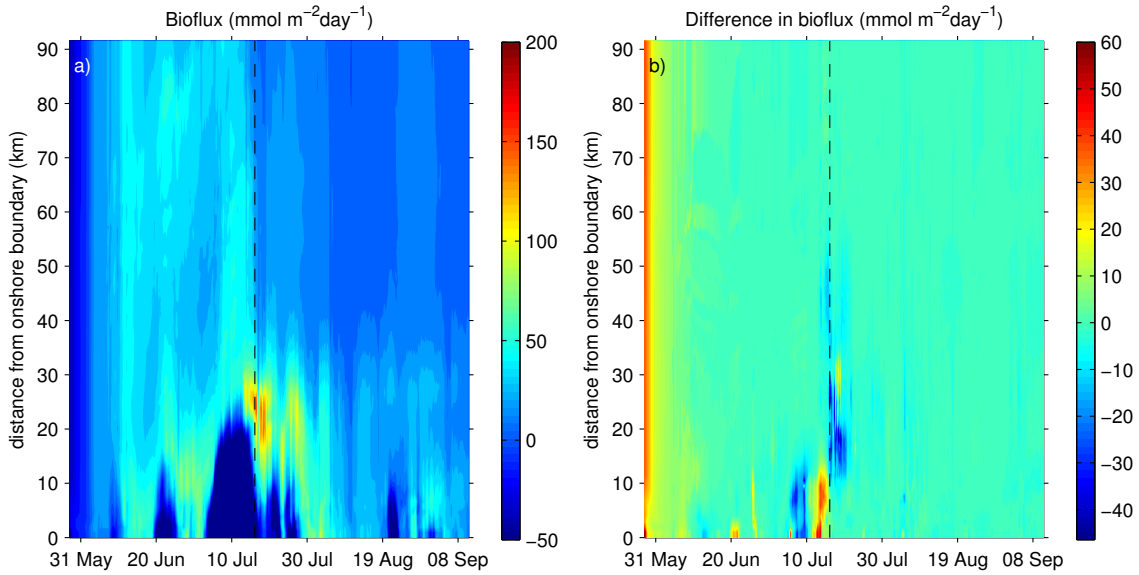

Figure A.3: Property plots within 90 km of the shore over the course of the second sensitivity run (1993) in which only oxygen was set to zero in the surface box. a) Bioflux in the sensitivity run, and b) difference between bioflux in the shallow shelf and sensitivity runs. Note the x-axis - this plot shows the spinup time (day 1 - 20), weighting time (day 20 - 50), and the remainder of the run after the spinup and weighting times. Black dotted line indicates the end of the spinup time plus the weighting time.

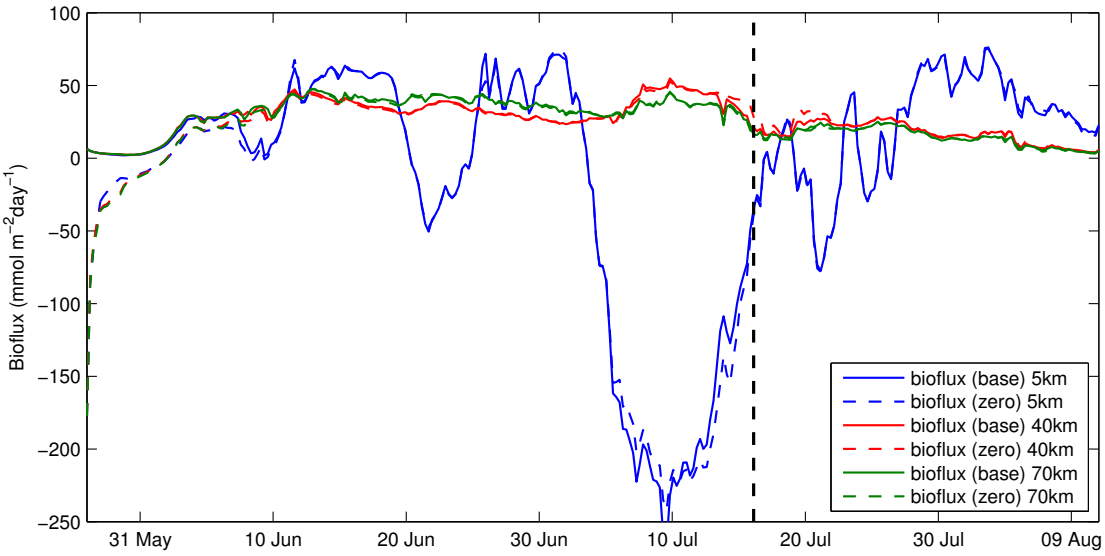

Figure A.4: Bioflux in the mixed layer over the course of the run in Figure A.3 and in the shallow shelf run at 5km offshore, 40 km offshore, and 70 km offshore. Black line represents the end of the spinup plus the weighting time.

Appendix B

Measurement of Argon

We measured Ar concentrations in duplicate at two stations and several depths off the west coast of Vancouver Island on 22-23 August 2013 for comparison to models results, Line P station P2 (48.6°N 126°W) and P4 (48.65°N 126.67°W). Discrete samples were collected from Niskin bottles through CO_2-flushed tubing into 180-mL pre-evacuated flasks until half full (Emerson et al., 1999). Samples were analyzed by isotope dilution with a ^{38}Ar spike using a variant of the method described in Hamme and Severinghaus (2007). Briefly, the water is equilibrated with the headspace and removed. Headspace gases are cryogenically processed and gettered to remove all but the noble gases, which are frozen into a long tube with a known amount of ^{38}Ar. We added He as a balance gas rather than N_2. Samples were analyzed for ^{40}Ar/^{38}Ar ratios against a standard of similar composition on a Finnigan MAT 253 isotope ratio mass spectrometer. Pooled standard deviation of the duplicates was 0.12% for these samples. Ar supersaturations are calculated as $\Delta Ar = (Ar_{meas}/Ar_{eq} - 1)$ and presented in percent, where Ar_{meas} is the measured Ar concentration and Ar_{eq} is the Ar concentration expected at equilibrium for that potential temperature and salinity (Hamme and Emerson, 2004).

Table B.1: Discrete argon measurements taken on 22-23 August, 2013 along with associated temperature, salinity, pressure, and station coordinates.

Latitude	Longitude	Pressure (db)	Temperature (°C)	Salinity (PSS-78)	[Ar] (μmol kg^{-1})	ΔAr (%)
48.60	-126.00	30.1	8.370	33.00	14.43	1.96
48.60	-126.00	30.1	8.370	33.00	14.43	1.97
48.60	-126.00	49.8	7.405	33.42	14.58	1.14
48.60	-126.00	49.8	7.405	33.42	14.60	1.29
48.60	-126.00	100.1	6.666	33.88	14.70	0.63
48.60	-126.00	100.1	6.666	33.88	14.73	0.81
48.65	-126.67	30.4	11.277	32.25	13.80	3.27
48.65	-126.67	30.4	11.277	32.25	13.79	3.21
48.65	-126.67	100.5	7.376	33.23	14.50	0.39
48.65	-126.67	100.5	7.376	33.23	14.54	0.63

Appendix C

Wide, narrow, and shallow shelf bathymetry

I performed three runs with different shelf bathymetries in order to test the sensitivity of my results to the width and depth of the continental shelf. One run has a 30 km wide shelf; one has a 70 km wide shelf; and the last has the same width shelf as the base run (40 km) but with a minimum depth of 39 m (as opposed to a 99 m minimum depth in the base run). There was little difference between the runs. While some small differences do exist, they are only at a few isolated points in NCP, bioflux and mixed layer depth (as a result I have not included these plots). The main difference seen is a small number of highly negative biological oxygen supersaturations in the shallow shelf run (Figure C.6), but these affect only 1% of the bioflux values.

The most notable thing about these runs is the percent difference in nitrate (Figures C.2, C.3, C.4). It should be noted that the concentration of mixed layer nitrate is small (median $[NO_3] = 0.15$ mmol m^{-3} in the base run) in the first place, and so a small change can cause a much larger percent difference than expected. In addition, most of the percent difference in nitrate appears to be on the same order as the other model data apart from a few select points. It appears that, at these points, the mixed layer is slightly deeper than in the base run, and that has perhaps entrained water that is high in nutrients. In the narrow shelf run, it appears that oxygen concentration is higher than in the base run during periods of high NCP, while it is lower in the wide shelf and shallow shelf runs. In almost all cases the percent difference is small (mean percent difference 43% for the shallow shelf run, 2.4% in the wide shelf run and 15% in the narrow shelf run) with large differences mainly seen at the beginning of

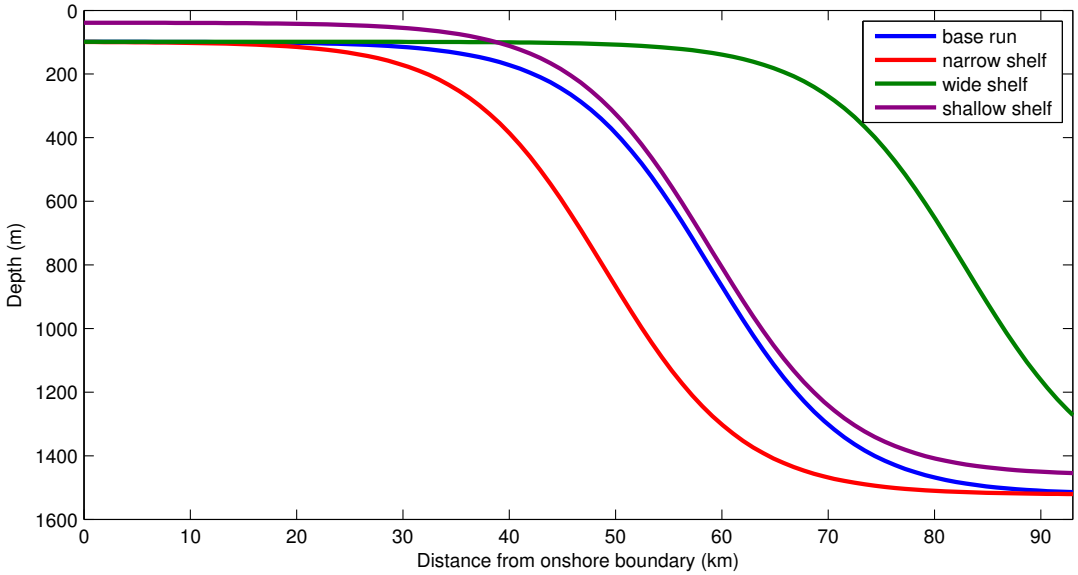

Figure C.1: Standard shelf bathymetry compared to narrow, wide and shallow shelves in these sensitivity runs.

the wide and narrow shelf runs, and at the end of the shallow shelf run. These periods in time and space correspond to the two largest blooms over the course of the run. The minimum oxygen concentrations (as marked by black crosses) in the narrow and wide shelf runs change by less than 1% between them and the base run at the same location. The minimum oxygen concentration in the shallow shelf run underestimates the base run by 53% at the same time and location (this time and location does not correspond to the minimum oxygen concentration in the base run). The percent differences between the minimum oxygen concentration for each run and the minimum oxygen concentration from the base run are 42% for the shallow shelf run, less than 1% for the wide shelf run, and 5% for the narrow shelf run. The differences in salinity and argon concentration are smaller yet, and appear to mostly be affected by slightly differing advection fluxes, as the stripes reflect horizontal advection oscillation periods (Kundu and Thomson, 1990).

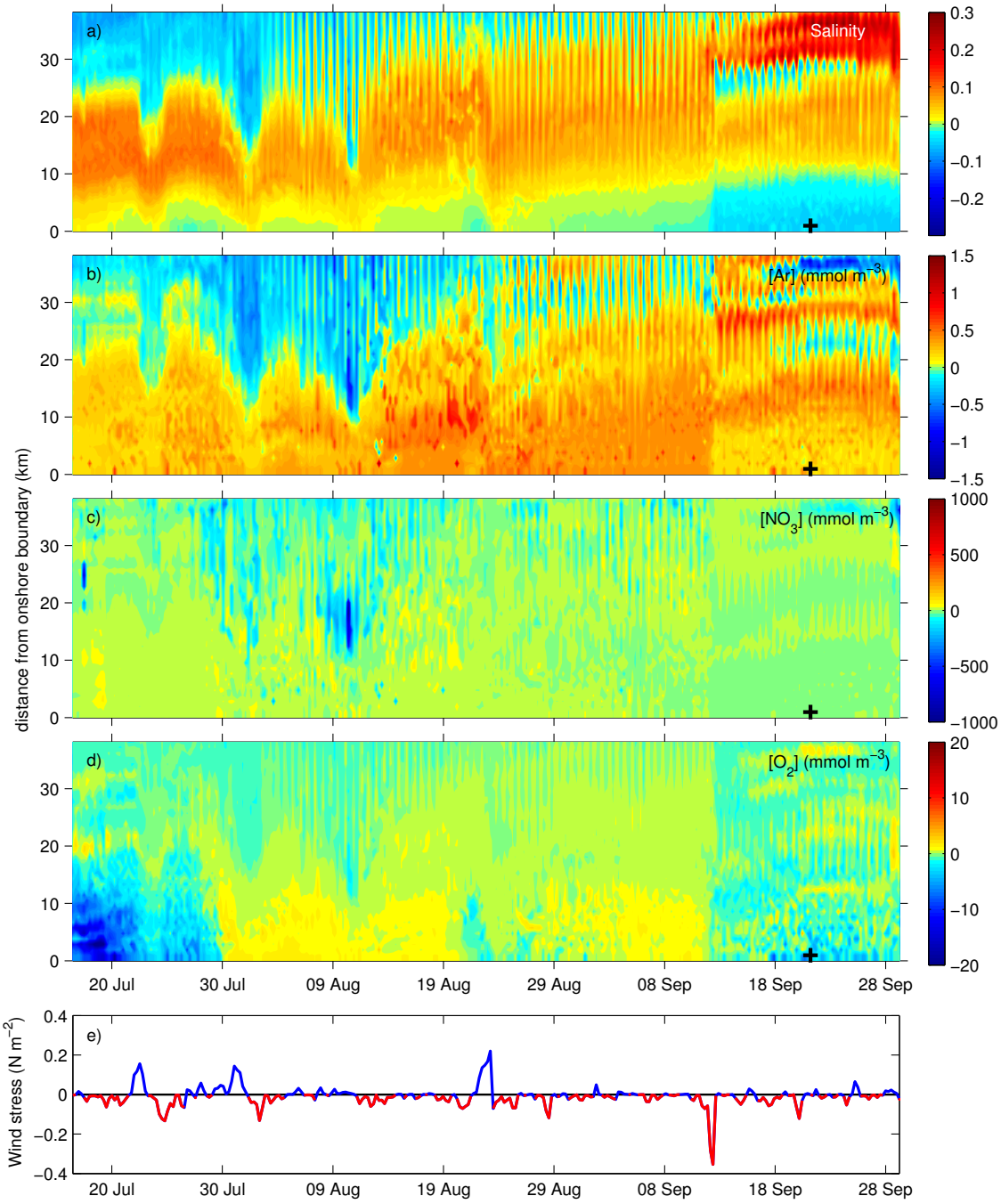

Figure C.2: Percent difference between the base run and the narrow shelf run in average a) salinity, b) argon, c) nitrate, and d) oxygen in the mixed layer over the shelf (distance offshore vs. time) and e) associated alongshore wind forcing (wind forcing vs. time) for a run with radiative and wind forcing from 1993. Negative wind forcing (red) is associated with upwelling, while positive wind forcing (blue) is associated with downwelling. Black crosses represent the minimum oxygen concentration in the mixed layer.

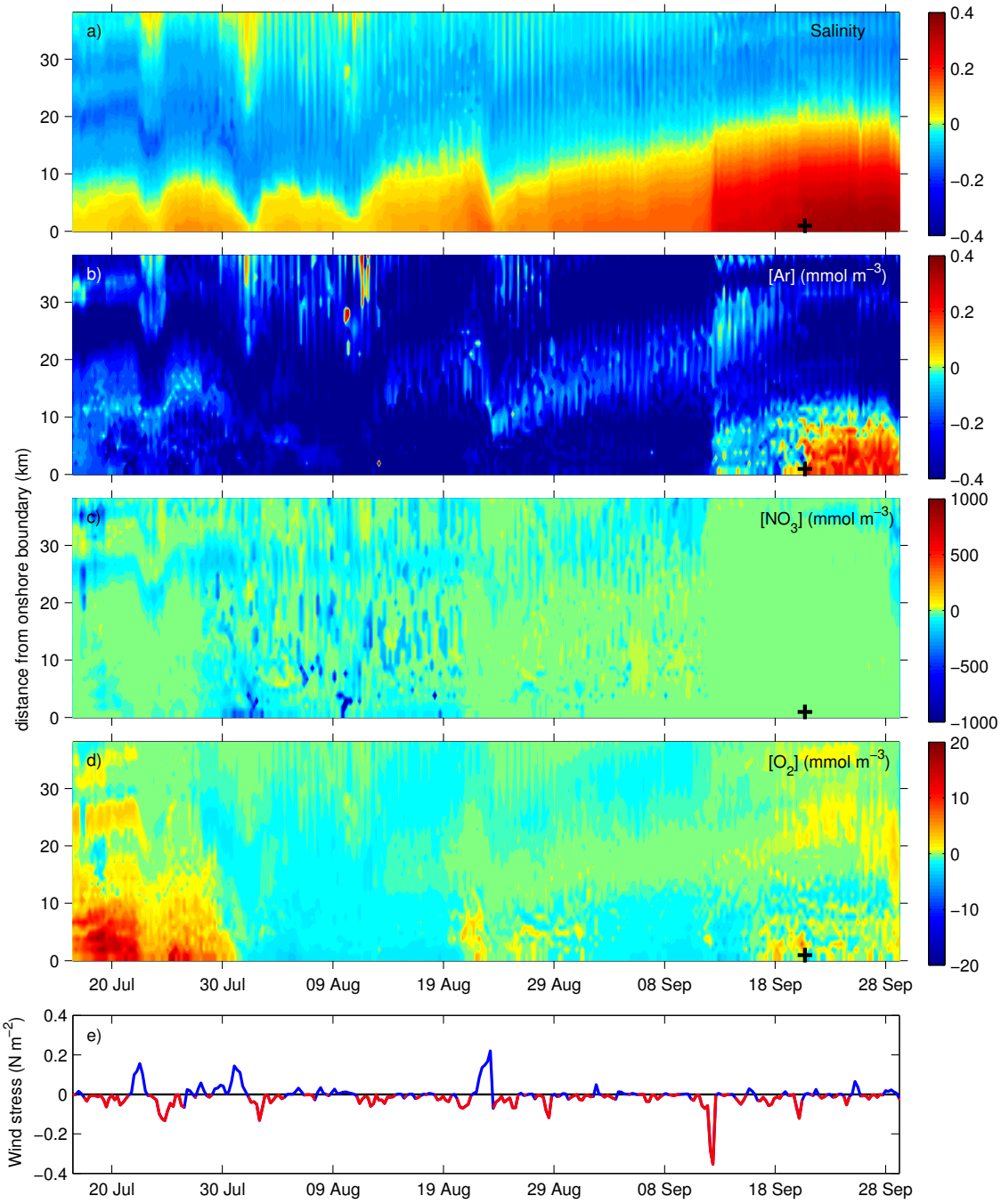

Figure C.3: Percent difference between the base run and the wide shelf run in average a) salinity, b) argon, c) nitrate, and d) oxygen in the mixed layer over the shelf (distance offshore vs. time) and e) associated alongshore wind forcing (wind forcing vs. time) for a run with radiative and wind forcing from 1993. Negative wind forcing (red) is associated with upwelling, while positive wind forcing (blue) is associated with downwelling. Black crosses represent the minimum oxygen concentration in the mixed layer.

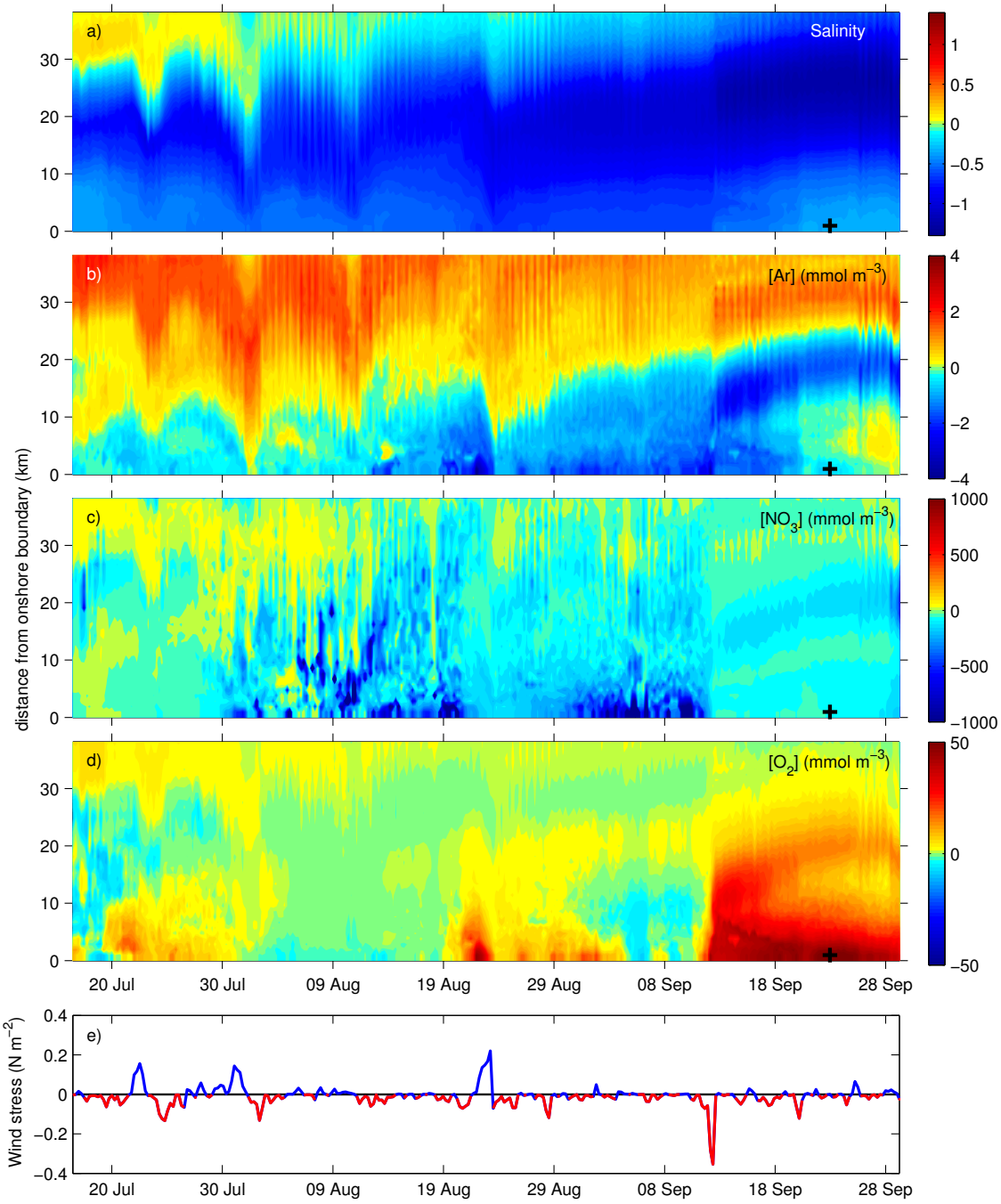

Figure C.4: Percent difference between the base run and the shallow shelf run in average a) salinity, b) argon, c) nitrate, and d) oxygen in the mixed layer over the shelf (distance offshore vs. time) and e) associated alongshore wind forcing (wind forcing vs. time) for a run with radiative and wind forcing from 1993. Negative wind forcing (red) is associated with upwelling, while positive wind forcing (blue) is associated with downwelling. Black crosses represent the minimum oxygen concentration in the mixed layer.

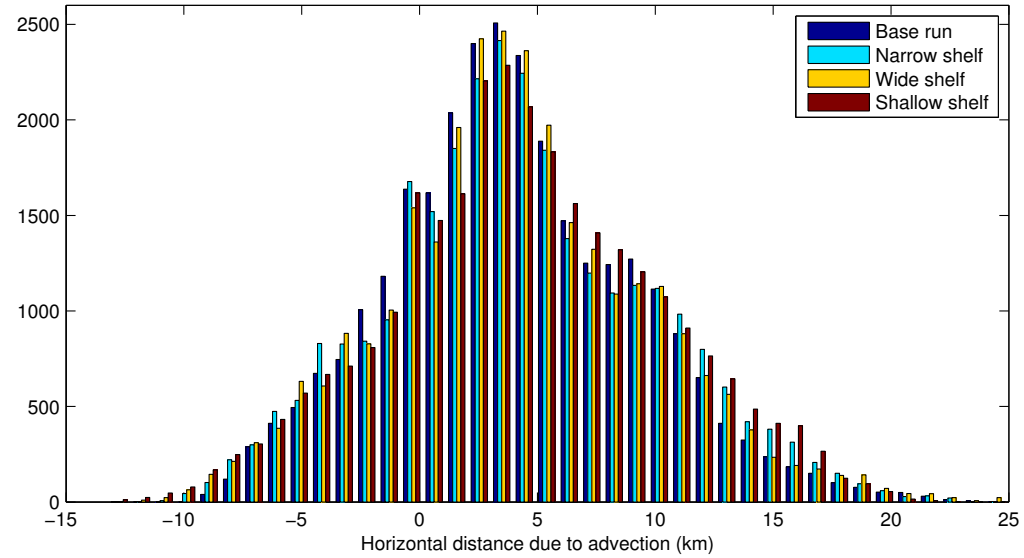

Figure C.5: Distribution of the horizontal distance water parcels are advected over the course of 9 days for each of the runs performed with different shelf widths or depth. Distance refers to the difference between the start and end point.

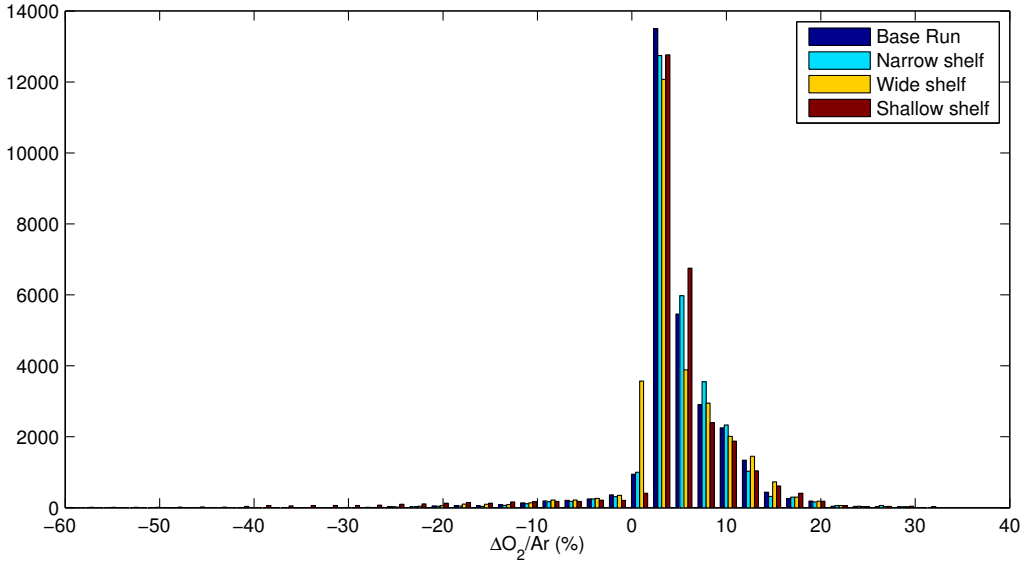

Figure C.6: Distribution of $\Delta O_2/Ar$ for each of the runs performed with different shelf widths or depth. Highly negative $\Delta O_2/Ar$ values are from the shallow shelf run.

Appendix D

2004 and 2008 wind and radiative forcing

To examine the generalization of my results, experiments were performed with wind forcing from two other years. Overall, 2004 had slightly more consistent upwelling-favourable wind forcing (Figure D.1). Though none of the peaks were as large as the upwelling-favourable wind event in mid-September 1993, there were more mid-sized upwelling-favourable wind events in 2004 (late July, mid-August, early September). There were also a couple of larger downwelling favourable wind events in mid September. 2008 was quite a strong year in terms of upwelling favourable wind forcing, most notably the fairly consistent upwelling favourable winds in mid to late July and early to mid September (Figure D.2). There are also large downwelling events in early August, late August, and late September.

Bioflux and NCP in both years show expected patterns based on the wind forcing with negative or low bioflux and highly positive NCP seen during upwelling favourable wind forcing (Figure D.3, D.4). The mean residence time with respect to gas exchange, using a 30 day weighting time for calculation of the weighted gas transfer velocity, is just less than 7 days for the runs using 2004 and 2008 forcing. The maximum distance a water parcel is advected during the residence time with respect to gas exchange for 2004 and 2008 are 37.5 km and 35.9 km, respectively, compared with 25 km in the base run. The longer advection distance in the 2004 run can be attributed to more consistent upwelling-favourable wind forcing, most notably in late July (Figure D.5). The longer advection distance in the 2008 run is more likely attributable to stronger wind forcing compared to the base run (Figure D.6).

The 2004 run has a few points where bioflux is higher than NCP; however most of these (based on values farther offshore than 37.5 km) are within the 20 mmol $m^{-2}day^{-1}$ range. These points are likely due to the areas in the middle of the run with consistently low windspeed, which would produce a pronounced bioflux lag effect. In addition, the mixed layer is highly variable in this run. At around 40 km offshore, bioflux overestimates NCP over the course of the run due to entrainment of oxygen produced below the mixed layer (Figure D.9). As there are few particularly large upwelling events, I do not see many high NCP values in the area offshore of 37.5 km (Figure D.7).

Apart from a few values where bioflux is higher than NCP (again mostly within the 20 mmol $m^{-2}day^{-1}$ range), most of the points in the 2008 run demonstrate underestimation of NCP by bioflux when upwelling is strong. Even past 34.9 km offshore, where the upwelling signal is expected to be largely erased, there are high NCP values which are significantly underestimated by bioflux, but since the residence time with respect to gas exchange only represents the time at which 63% of oxygen will be ventilated, effects of the upwelling plume will still occasionally be seen (Figure D.8). This result is expected in a year with strong upwelling-favourable wind forcing. When making observations during strong upwelling years or events, it should be noted that bioflux significantly underestimates NCP.

In 2004, cumulative bioflux drastically underestimates cumulative NCP at 5 km offshore which is expected based on the numerous but smaller upwelling events over the course of the run (Figure D.9). In fact, cumulative bioflux in this location is comparatively close to zero over the whole run. Offshore, cumulative NCP and bioflux are fairly evenly matched, with bioflux overestimating NCP by a small amount at 70 km offshore over the course of the run where there is overall positive entrainment and vertical diffusion into the mixed layer causing an overestimation of NCP by bioflux. The mixed layer is fairly dynamic, changing quite rapidly. The entrainment term is overall negative at 40 km offshore due to detrainment of oxygen from the mixed layer. The most onshore location shows that the water below the mixed layer is quite undersaturated, causing more highly negative entrainment and vertical diffusion terms. The percent difference between the minimum oxygen concentration and the minimum oxygen concentration from the base run is 4%.

In 2008, the entrainment term and the vertical diffusion term remain similar throughout the run at 40 km offshore as in the base run (Figure D.10). At 70 km offshore, the entrainment term becomes more negative, likely due to detrainment

around the end of July. At 5 km offshore, the entrainment term is variable due to the rapid changing of the mixed layer depth, and overall negative due to the entrainment of water undersaturated in oxygen. The vertical diffusion term at 5 km offshore is overall negative for the same reasons. The bioflux term strongly underestimates NCP at this location. The mixed layer is often undersaturated causing an influx of oxygen to the mixed layer. There is some oxygen leaving the mixed layer over the month of August when windspeeds are relatively low. The percent difference between the minimum oxygen concentration and the minimum oxygen concentration from the base run is 45% with 2008 having the lower concentration.

Both 2004 and 2008 have fairly similar distributions of $\Delta O_2/Ar$ to the base run with the largest peak at 2-3%. The 2008 run has a few values which are highly negative as expected in a year with very strong upwelling-favourable wind forcing (Figure D.11).

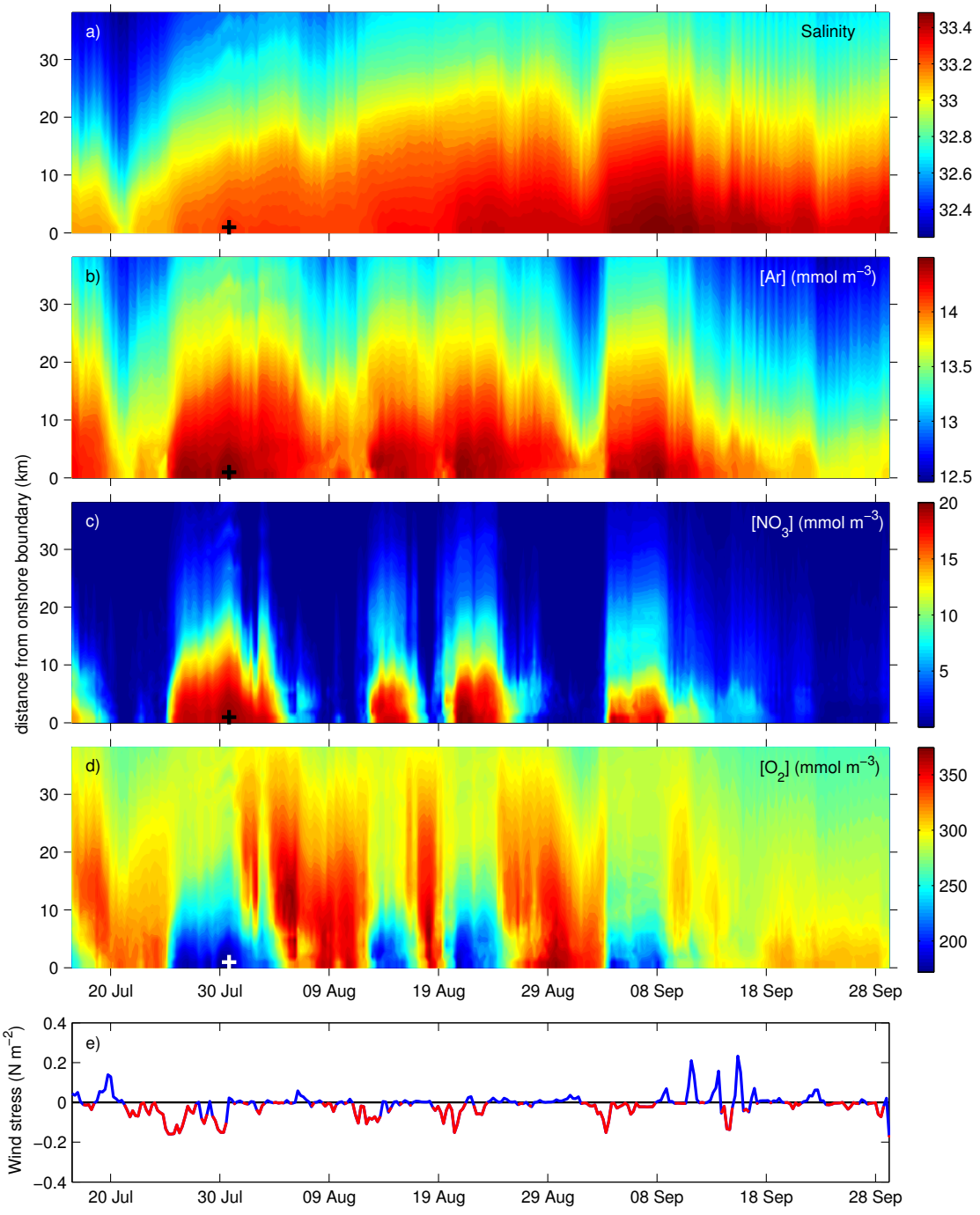

Figure D.1: Average a) salinity, b) argon, c) nitrate, and d) oxygen in the mixed layer over the shelf (distance offshore vs. time) and e) associated alongshore wind forcing (wind forcing vs. time) for a run with wind and radiative forcing from 2004. Negative wind forcing (red) is associated with upwelling, while positive wind forcing (blue) is associated with downwelling. Crosses mark the point of lowest oxygen concentration.

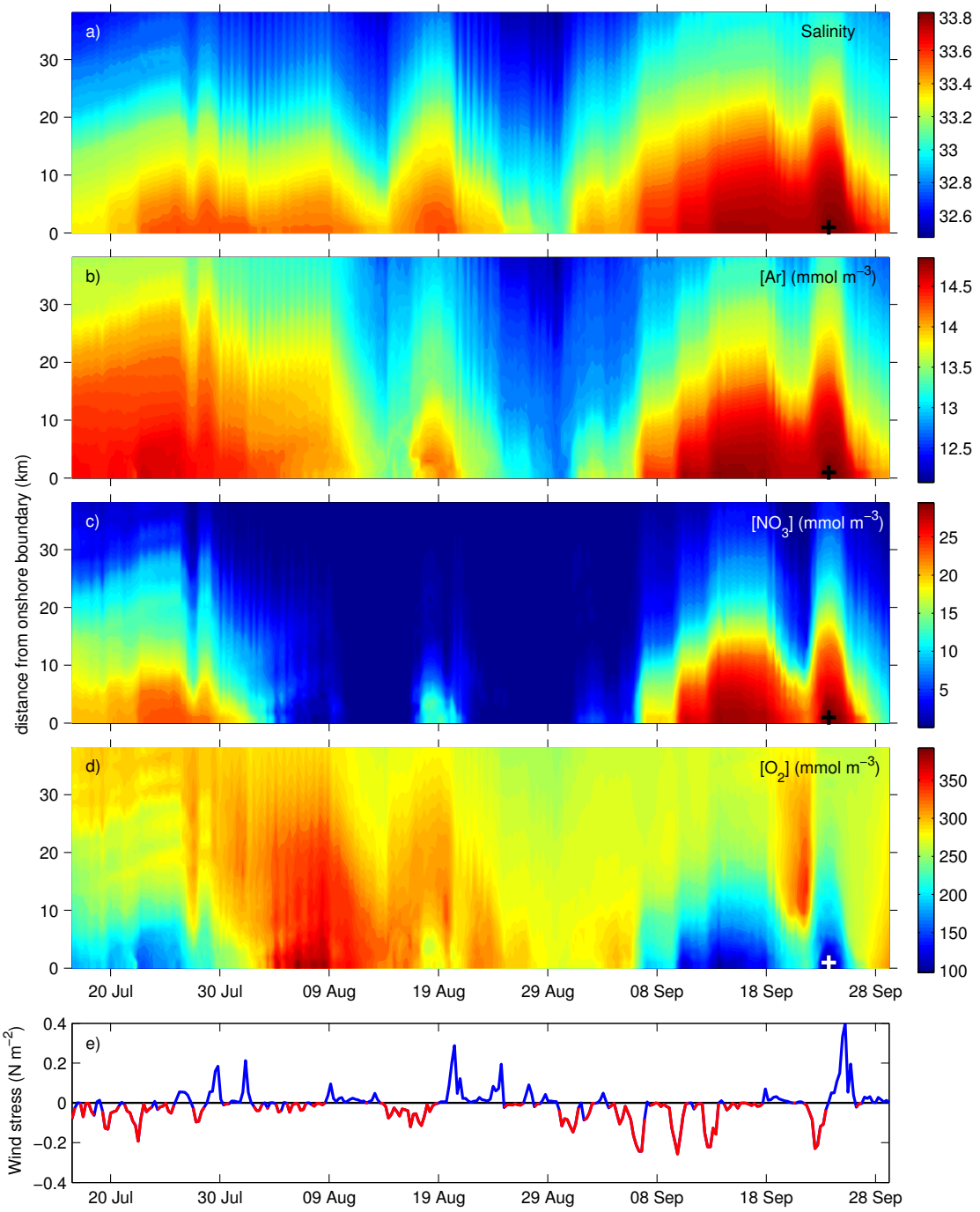

Figure D.2: Average a) salinity, b) argon, c) nitrate, and d) oxygen in the mixed layer over the shelf (distance offshore vs. time) and e) associated alongshore wind forcing (wind forcing vs. time) for a run with wind and radiative forcing from 2008. Negative wind forcing (red) is associated with upwelling, while positive wind forcing (blue) is associated with downwelling. Crosses mark the point of lowest oxygen concentration.

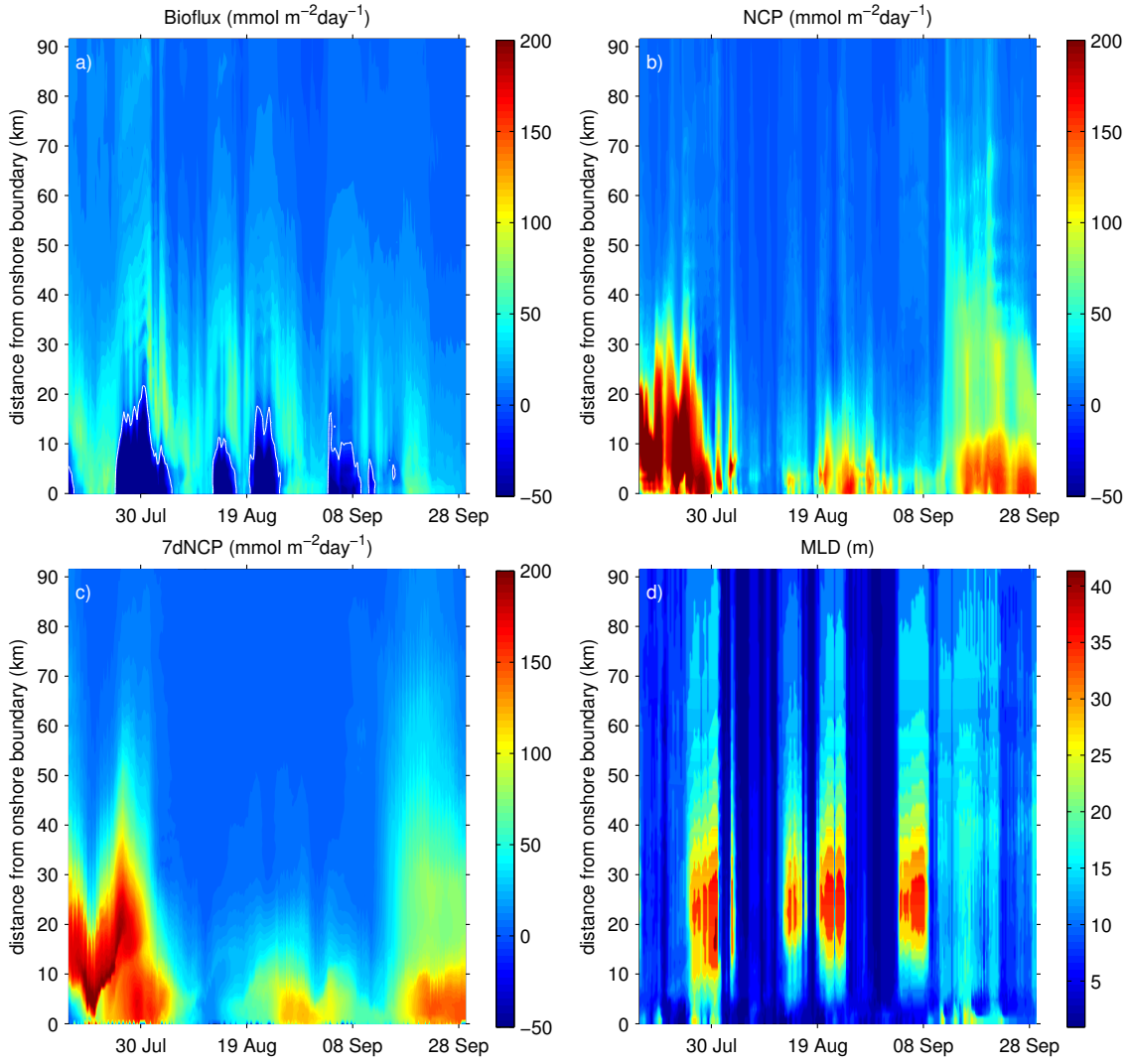

Figure D.3: Property plots within 90 km of the shore over the course of the run using 2004 forcing. a) Bioflux (white contours represent the division between positive and negative values), b) instantaneous mixed layer NCP, c) mixed layer NCP averaged over the previous 7 days following the Langrangian advection of the water parcel, and d) mixed layer depth.

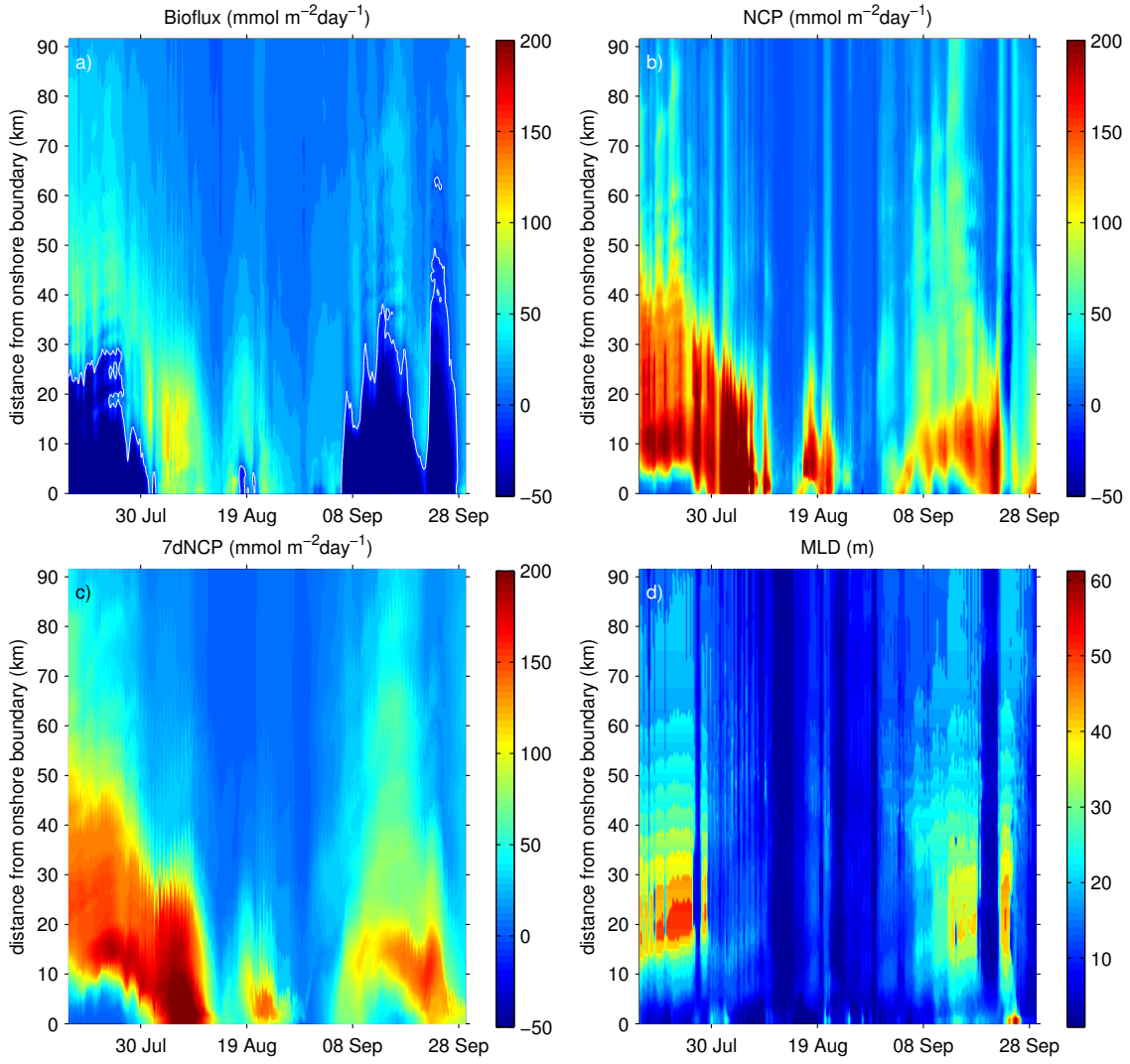

Figure D.4: Property plots within 90 km of the shore over the course of the run using 2008 forcing. a) Bioflux (white contours represent the division between positive and negative values), b) instantaneous mixed layer NCP, c) mixed layer NCP averaged over the previous 7 days following the Langrangian advection of the water parcel, and d) mixed layer depth.

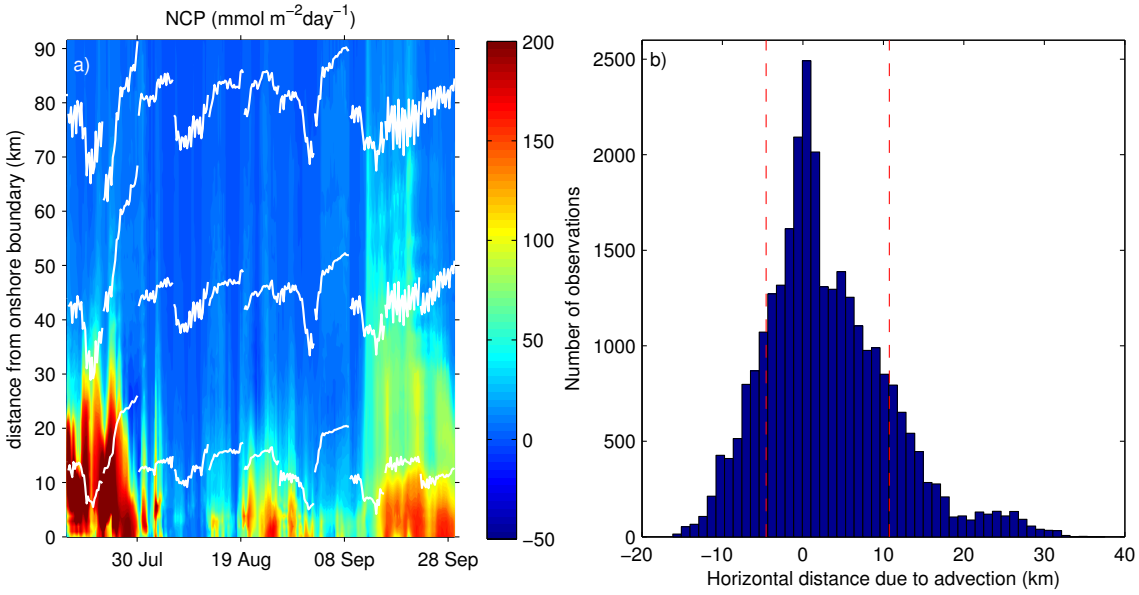

Figure D.5: 2004 forcing run: a) Instantaneous NCP with advection tracks showing the horizontal advection of the water in the mixed layer over 7 days beginning at either 10, 40, and 70 km offshore. Advection tracks begin every 7 days at each distance offshore. b) Distribution of the horizontal distance water parcels are advected over the course of 7 days. Distance refers to the difference between the start and end point. 70% of the data are contained between the red dashed lines.

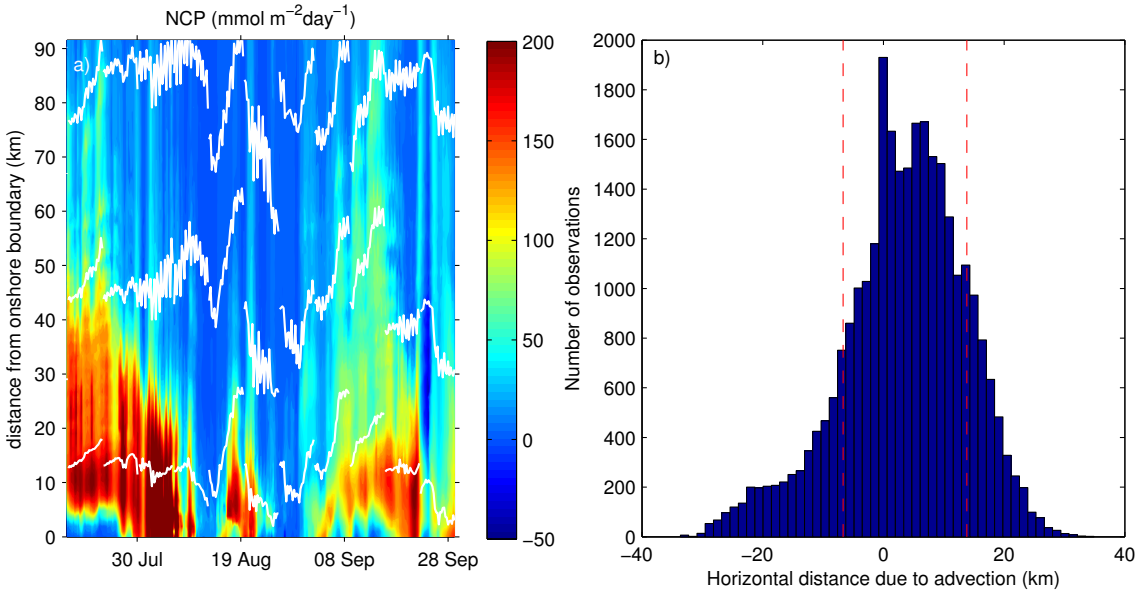

Figure D.6: 2008 forcing run: a) Instantaneous NCP with advection tracks showing the horizontal advection of the water in the mixed layer over 7 days beginning at either 10, 40, and 70 km offshore. Advection tracks begin every 7 days at each distance offshore. b) Distribution of the horizontal distance water parcels are advected over the course of 7 days. Distance refers to the difference between the start and end point. 70% of the data are contained between the red dashed lines.

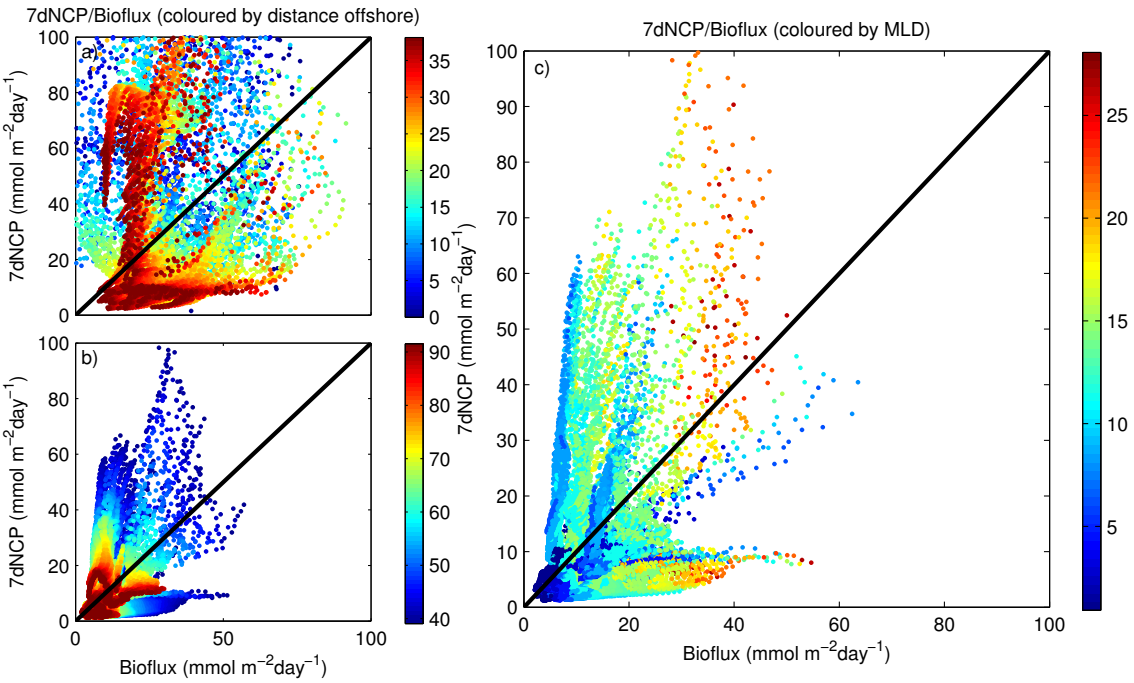

Figure D.7: 2004 forcing run: Bioflux plotted vs 7dNCP a) onshore (1-40 km) and b) offshore (40-90 km) coloured by distance offshore. c) Bioflux plotted vs 7dNCP 38-90 km offshore coloured by MLD. The black line represents the 1:1 relationship between bioflux and 7dNCP in all plots.

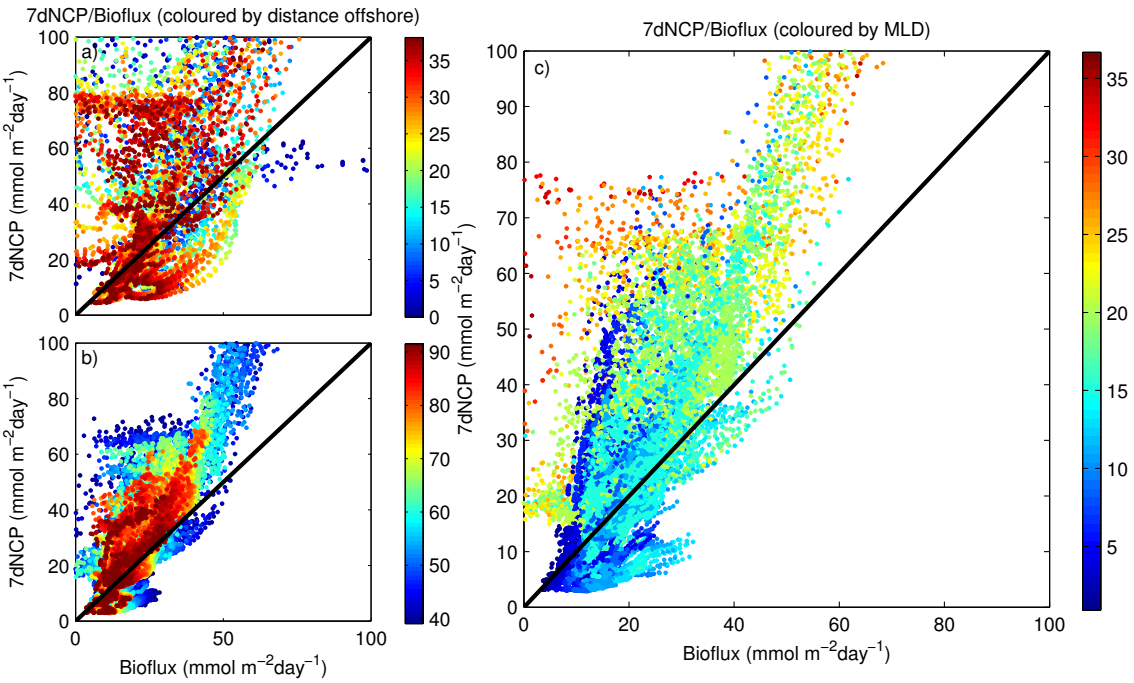

Figure D.8: 2008 forcing run: Bioflux plotted vs 7dNCP a) onshore (1-40 km) and b) offshore (40-90 km) coloured by distance offshore. c) Bioflux plotted vs 7dNCP 35-90 km offshore coloured by MLD. The black line represents the 1:1 relationship between bioflux and 7dNCP in all plots.

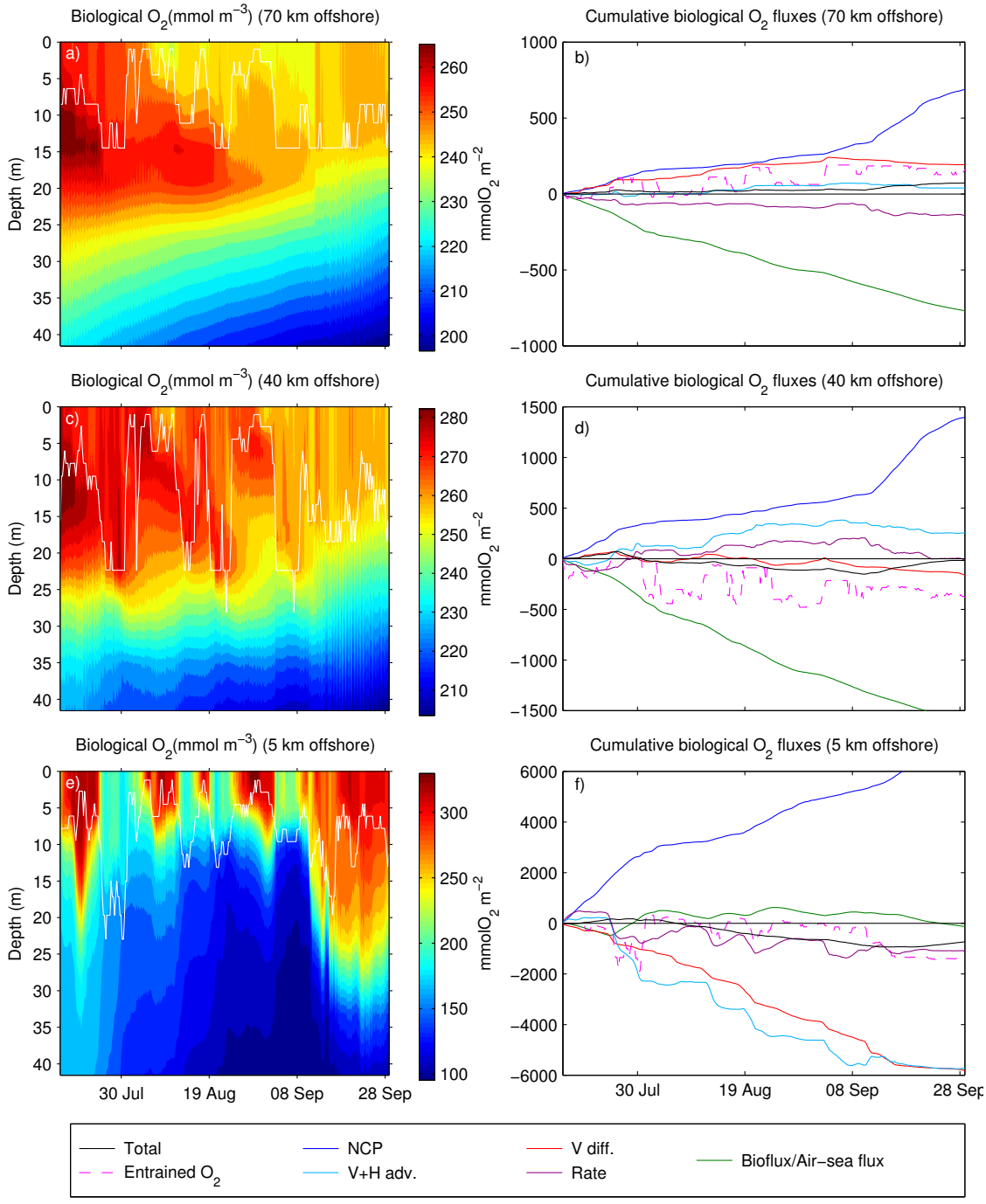

Figure D.9: 2004 forcing run: Biological oxygen concentration and mixed layer depth (white line) for 70 km offshore (a), 40 km offshore (c), and 5 km offshore (e). Cumulative O_2 fluxes for 70 km offshore (b), 40 km offshore (d), and 5 km offshore (f).

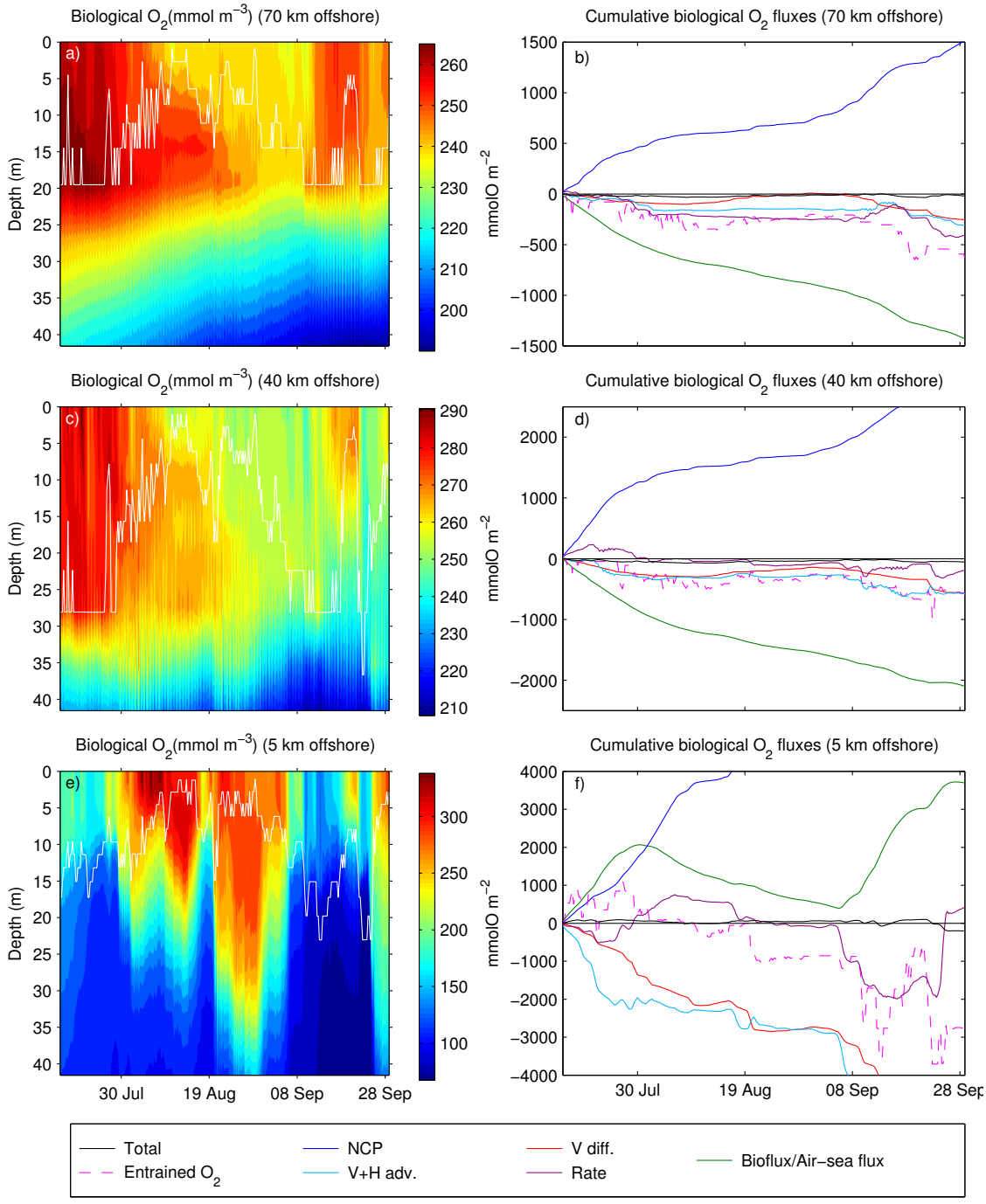

Figure D.10: 2008 forcing run: Biological oxygen concentration and mixed layer depth (white line) for 70 km offshore (a), 40 km offshore (c), and 5 km offshore (e). Cumulative O_2 fluxes for 70 km offshore (b), 40 km offshore (d), and 5 km offshore (f).

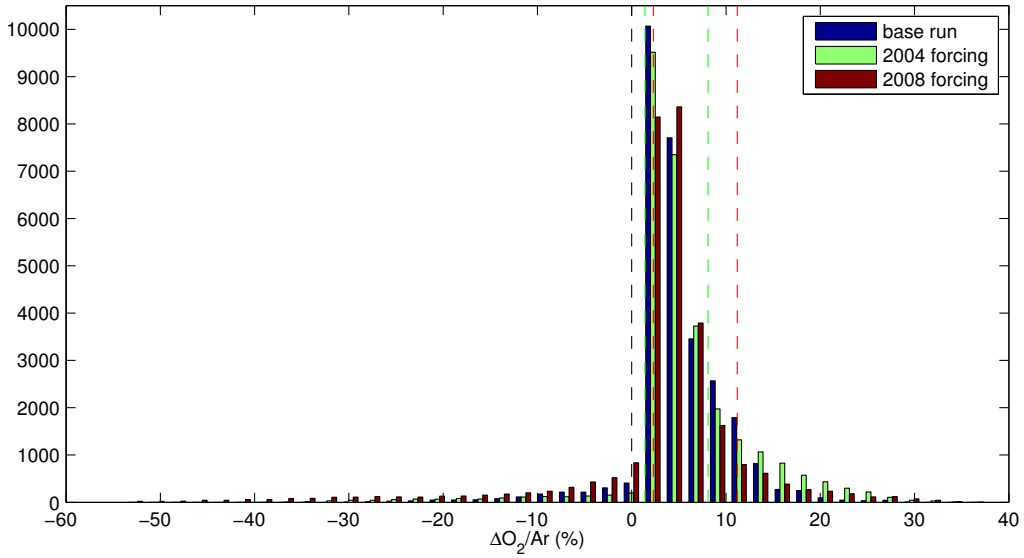

Figure D.11: Distribution of $\Delta O_2/Ar$ for the 2004 and 2008 forcing runs. Black dashed line marks 0. 70% of the data are contained between the green dashed lines (2004) and the red dashed lines (2008). Highly negative $\Delta O_2/Ar$ values are from the 2008 run.